77±32% for pitavastatin, and 76±39% for cerivastatin) or LY294002 (69±23% for pravastatin, 70±27% for pitavastatin, and 68±21% for cerivastatin).

Discussion

The present study demonstrates that several statins provide immediate infarct limitation of different magnitudes and at different optimal doses. Our results also suggest that activation of ecto-5′-nucleotidase through the activation of PI3-K after ischemia was involved in this cardioprotective mechanism of statins.

Cholesterol-Lowering Effects and Immediate Infarct Limitation of Statins

In this study, we set the doses of statins in line with their clinical cholesterol-lowering properties. In Japan, the standard clinical doses to obtain a 20% to 30% reduction of total plasma cholesterol levels were 10 mg/d for pravastatin, 2 mg/d for pitavastatin, and 0.15 mg/d for cerivastatin. Our preliminary trials in the same dog model revealed that a single intravenous injection of 0.2 mg/kg pravastatin, 0.1 mg/kg pitavastatin, or 5 μg/kg cerivastatin approximated the clinical cholesterol-lowering dose based on the maximal plasma concentration of each statin (data not shown). Because (1) the maximal infarct limitation was achieved by a higher dose of pravastatin than the clinical dose, whereas the dose was similar to the clinical dose for pitavastatin and lower for cerivastatin, and (2) these statins showed early cardioprotection within 2 hours of administration in this model, it is strongly suggested that the magnitude of immediate infarct limitation by each statin is not correlated with its cholesterol-lowering effect.

Existence of Optimal Cardioprotective Doses for Each Statin

In the present report, we have directly shown that pitavastatin has the optimal dose to reduce infarct size. Obviously, there is also an optimal dose for cerivastatin under the lowest dose we tried, because infarct size with far lower doses of cerivastatin near zero will converge with those of control levels. In the case of pravastatin, our additional experiment, within the limitation with regard to the total amount of the drug we could obtain, showed that 100 mg/kg pravastatin administered in the same manner as in protocol 1 exerted similar (but a slightly weaker) magnitude of reducing infarct size (20.9±4.5%, n=5) compared with that achieved with 10 mg/kg of this agent. Although we could not show direct evidence in this case, it would at least not deny the possibility for the existence of an optimal dose of pravastatin. Furthermore, other reports also showed the existence of an optimal dose of atorvastatin for infarct limitation[9] or of simvastatin for PI3-K activation.[8] Taken together, the existence of optimal doses should be ubiquitous among all (or at least all hydrophobic) statins.

Although direct exhibition of the reason for this phenomenon remains unclear in this study, there might be some reasons to regulate the respective optimal windows for each statin, eg, differences in the ability to attenuate inflammatory response[20] or in the potency of direct absorption into cellular membrane to modulate intracellular signaling systems. In addition, our present finding that infarct limitation completely paralleled the activation of PI3-K leads us to hypothesize that the lesser effects by the higher doses of statins should be regulated upstream of PI3-K. One possibility is that all hydrophobic statins can dose-dependently activate apoptosis-related signals,[21] which might also explain the wide range of higher cardioprotective doses for pravastatin specifically. Finally, additional studies will need to be performed to obtain direct evidence.

Cardioprotective Mechanisms

Our observations that (1) activation of PI3-K and ecto-5′-nucleotidase was coincident with a substantial limitation of infarct size, (2) either wortmannin or AMP-CP abolished cardioprotection by all 3 statins, (3) different PI3-K inhibitors at reperfusion actually inhibited PI3-K activity (Figure 4) and subsequently reduced ecto-5′-nucleotidase activity (Figure 3), and (4) our preliminary documentation that PI3-K inhibition by either wortmannin of LY294002 before ischemia did not abolish the infarct limitation by statins in the present study (n=4 or 5, data not shown), together suggest that infarct limitation in this model was linked to the activation of PI3-K during reperfusion, not before ischemia, followed by ecto-5′-nucleotidase activation.

In this study, we did not determine the exact mechanism of how PI3-K activates ecto-5′-nucleotidase. Although we have previously reported that phosphorylation of ecto-5′-nucleotidase might be crucial,[22] other mechanisms may also be involved, such as endocytotic turnover.[17] In addition, although we did not evaluate real-time regional myocardial production of adenosine in each group, treatment with a potent adenosine receptor antagonist (8-SPT) during reperfusion also blunted infarct limitation by statins along with the inhibition of ecto-5′-nucleotidase, further suggesting that cardioprotection against ischemia-reperfusion injury via ecto-5′-nucleotidase activation might be mediated by an increase of adenosine, the main product of ecto-5′-nucleotidase.[11,13,22] However, other implicated mechanism of enhanced activation of the adenosine receptor (eg, increased receptor sensitivity) should be determined by future studies.

Possible Link Between Cardioprotection by Adenosine and NO

Previous studies support our present findings that statins rapidly activate the PI3-K/Akt pathway,[8,9] and we obtained another preliminary finding that the cotreatment with N^{ω}-nitro-L-arginine methyl ester (10 $\mu g \cdot kg^{-1} \cdot min^{-1}$) in the same manner as in protocol 1, which we confirmed did not affect baseline infarct size in the present model,[23] blunted the infarct limitation by pravastatin (36.8±4.1%, n=7), pitavastatin (39.9±3.9%, n=6), and cerivastatin (42.6±4.6%, n=5). Therefore, there is a possibility that ecto-5′-nucleotidase and NO act in series to cause statin-induced cardioprotection.

Although elucidation of a direct effect should be the focus of future studies, there are at least 2 lines of evidence to support the explanation that adenosine and NO synergistically caused infarct limitation in this study. First, NO directly exerts cardioprotection[24]: NO inhibits cell-to-cell adhesion,

such as that between platelets[25] or between neutrophils and endothelial cells,[26,27] by reducing expression of P-selectin,[27] E-selectin, and intercellular adhesion molecule-1,[28] which leads to attenuation of the inflammatory response[22,24,25] or protects against ischemia-reperfusion injury.[25–28] In addition, NO is reported to inhibit caspase-3 activity and to block apoptosis of cardiac myocytes.[29] On the other hand, adenosine also rescues injured myocardium through activating adenosine receptors.[13,30–32] Either administration of adenosine or enhancement of endogenous adenosine release during reperfusion after sustained ischemia limits infarct size.[13,17] We and others have shown that (1) adenosine receptor (A_1 and A_2) activation improves contractile dysfunction after reperfusion,[14] (2) inhibition of norepinephrine release from the presynaptic vesicles and attenuation of calcium influx occur through the A_1 receptor and the coupled inhibitory G protein,[33,34] (3) inhibition of platelet aggregation and leukocyte activation occurs through the A_2 receptor and the coupled stimulatory G protein,[34–36] and (4) activation of extracellular signal regulated kinase, one of the reperfusion injury survival kinase pathways,[37] takes place during reperfusion through the A_3 receptor.[38] Therefore, either adenosine or NO similarly and potentially protects injured myocardium through multiple pathways.

Second, recent articles have shown that either adenosine[38–40] or NO[41] can reactivate PI3-K downstream. However, increasing the production of both agents is known to negatively regulate further increases of production of these molecules,[42,43] suggesting the requirement of both pathways to confer sufficient cardioprotection in the physiological system. Taking all of these together, it is likely that adenosine and NO synergistically confer the statin-derived immediate cardioprotection shown in this study.

In conclusion, our findings suggest the cellular mechanism by which statins attenuate myocardial injury, which may indicate the possibility of acute protective therapies for ischemia and associated myocardial stresses.

Acknowledgments

This study was supported by grants on the Human Genome, Tissue Engineering and Food Biotechnology (H13-Genome-11) and grants on Comprehensive Research on Aging and Health (H13-21seiki[seikatsu]-23) in Health and Labor Sciences Research from the Ministry of Health, Labor and Welfare; a grant-in-aid for Scientific Research from the Ministry of Education, Culture, Sports, Science and Technology of Japan; and in part by a grant-in-aid for JSPS fellows from the Japan Society for the Promotion of Science and the Japan Heart Foundation.

References

1. Goldstein JL, Brown MS. Regulation of the mevalonate pathway. *Nature*. 1990;343:425–430.
2. Sacks FM, Pfeffer MA, Moye LA, et al. The effect of pravastatin on coronary events after myocardial infarction in patients with average cholesterol levels: Cholesterol and Recurrent Events Trial investigators. *N Engl J Med*. 1996;335:1001–1009.
3. LIPID Study Group. Prevention of cardiovascular events and death with pravastatin in patients with coronary heart disease and a broad range of initial cholesterol levels: the Long-Term Intervention with Pravastatin in Ischaemic Disease (LIPID) Study Group. *N Engl J Med*. 1998;339:1349–1357.
4. 4S Study Group. Randomized trial of cholesterol lowering in 4444 patients with coronary heart disease: the Scandinavian Simvastatin Survival Study (4S). *Lancet*. 1994;344:1383–1389.
5. Downs JR, Clearfield M, Weis S, et al. Primary prevention of acute coronary events with lovastatin in men and women with average cholesterol levels: results of AFCAPS/TexCAPS: Air Force/Texas Coronary Atherosclerosis Prevention Study. *JAMA*. 1998;279:1615–1622.
6. Lefer AM, Campbell B, Shin YK, et al. Simvastatin preserves the ischemic-reperfused myocardium in normocholesterolemic rat hearts. *Circulation*. 1999;100:178–184.
7. Ikeda Y, Young LH, Lefer AM. Rosuvastatin, a new HMG-CoA reductase inhibitor, protects ischemic reperfused myocardium in normocholesterolemic rats. *J Cardiovasc Pharmacol*. 2003;41:649–656.
8. Kureishi Y, Luo Z, Shiojima I, et al. The HMG-CoA reductase inhibitor simvastatin activates the protein kinase Akt and promotes angiogenesis in normocholesterolemic animals. *Nat Med*. 2000;6:1004–1010.
9. Bell RM, Yellon DM. Atorvastatin, administered at the onset of reperfusion, and independent of lipid lowering, protects the myocardium by up-regulating a pro-survival pathway. *J Am Coll Cardiol*. 2003;41:508–515.
10. Simoncini T, Genazzani AR, Liao JK. Nongenomic mechanisms of endothelial nitric oxide synthase activation by the selective estrogen receptor modulator raloxifene. *Circulation*. 2002;105:1368–1373.
11. Ledoux S, Laouari D, Essig M, et al. Lovastatin enhances ecto-5′-nucleotidase activity and cell surface expression in endothelial cells: implication of rho-family GTPases. *Circ Res*. 2002;90:420–427.
12. Kitakaze M, Hori M, Morioka T, et al. α$_1$-Adrenoceptor activation mediates the infarct size-limiting effect of ischemic preconditioning through augmentation of 5′-nucleotidase activity. *J Clin Invest*. 1994;93:2197–2205.
13. Kitakaze M, Minamino T, Node K, et al. Adenosine and cardioprotection in the diseased heart. *Jpn Circ J*. 1999;63:231–243.
14. Tuma PL, Finnegan CM, Yi JH, et al. Evidence for apical endocytosis in polarized hepatic cells: phosphoinositide 3-kinase inhibitors lead to the lysosomal accumulation of resident apical plasma membrane proteins. *J Cell Biol*. 1999;145:1089–1102.
15. Kitakaze M, Node K, Minamino T, et al. Role of activation of protein kinase C in the infarct size-limiting effect of ischemic preconditioning through activation of ecto-5′-nucleotidase. *Circulation*. 1996;93:781–791.
16. Sanada S, Kitakaze M, Papst PJ, et al. Role of phasic dynamism of p38 mitogen-activated protein kinase activation in the ischemic preconditioning on the canine heart. *Circ Res*. 2001;88:175–180.
17. Kitakaze M, Minamino T, Funaya H, et al. Vesnarinone limits infarct size via adenosine-dependent mechanisms in the canine heart. *Circulation*. 1997;95:2108–2114.
18. Node K, Kitakaze M, Minamino T, et al. Activation of ecto-5′-nucleotidase by protein kinase C and its role in ischaemic tolerance in the canine heart. *Br J Pharmacol*. 1997;120:273–281.
19. Ogita H, Node K, Asanuma H, et al. Raloxifene improves coronary perfusion, cardiac contractility and myocardial metabolism in the ischemic heart: role of phosphatidylinositol 3-kinase/Akt pathway. *J Cardiovasc Pharmacol*. 2004;43:821–829.
20. Hilgendorff A, Muth H, Parviz B, et al. Statins differ in their ability to block NF-κB activation in human blood monocytes. *Int J Clin Pharmacol Ther*. 2003;41:397–401.
21. Kaneta S, Satoh K, Kano S, et al. All hydrophobic HMG-CoA reductase inhibitors induce apoptotic death in rat pulmonary vein endothelial cells. *Atherosclerosis*. 2003;170:237–243.
22. Kitakaze M, Minamino T, Node K, et al. Activation of ecto-5′-nucleotidase and cardioprotection of ischemic preconditioning. *Basic Res Cardiol*. 1996;91:23–26.
23. Asanuma H, Kitakaze M, Funaya H, et al. Nifedipine limits infarct size via NO-dependent mechanisms in dogs. *Basic Res Cardiol*. 2001;96:497–505.
24. Lefer AM, Lefer DJ. Nitric oxide, II: nitric oxide protects in intestinal inflammation. *Am J Physiol*. 1999;276:G572–G575.
25. Massberg S, Sausbier M, Klatt P, et al. Increased adhesion and aggregation of platelets lacking cyclic guanosine 3′,5′-monophosphate kinase I. *J Exp Med*. 1999;189:1255–1264.
26. Agullo L, Garcia-Dorado D, Inserte J, et al. L-Arginine limits myocardial cell death secondary to hypoxia-reoxygenation by a cGMP-dependent mechanism. *Am J Physiol*. 1999;276:H1574–H1580.

27. Jordan JE, Zhao ZQ, Vinten-Johansen J. The role of neutrophils in myocardial ischemia-reperfusion injury. *Cardiovasc Res*. 1999;43: 860–878.
28. Buras JA, Stahl GL, Svoboda KK, et al. Hyperbaric oxygen downregulates ICAM-1 expression induced by hypoxia and hypoglycemia: the role of NOS. *Am J Physiol Cell Physiol*. 2000;278:C292–C302.
29. Weiland U, Haendeler J, Ihling C, et al. Inhibition of endogenous nitric oxide synthase potentiates ischemia-reperfusion–induced myocardial apoptosis via a caspase-3 dependent pathway. *Cardiovasc Res*. 2000;45: 671–678.
30. Dorheim TA, Hoffman A, Van Wylen DG, et al. Enhanced interstitial fluid adenosine attenuates myocardial stunning. *Surgery*. 1991;110: 136–145.
31. Babbitt DG, Virmani R, Vildibill HD Jr, et al. Intracoronary adenosine administration during reperfusion following 3 hours of ischemia: effects on infarct size, ventricular function, and regional myocardial blood flow. *Am Heart J*. 1990;120:808–818.
32. Norton ED, Jackson EK, Virmani R, et al. Effect of intravenous adenosine on myocardial reperfusion injury in a model with low myocardial collateral blood flow. *Am Heart J*. 1991;122:1283–1291.
33. Richardt G, Waas W, Kranzhofer R, et al. Adenosine inhibits exocytotic release of endogenous noradrenaline in rat heart: a protective mechanism in early myocardial ischemia. *Circ Res*. 1987;61:117–123.
34. Sato H, Hori M, Kitakaze M, et al. Endogenous adenosine blunts β-adrenoceptor–mediated inotropic response in hypoperfused canine myocardium. *Circulation*. 1992;85:1594–1603.
35. Cronstein BN, Levin RI, Belanoff J, et al. Adenosine: an endogenous inhibitor of neutrophil-mediated injury to endothelial cells. *J Clin Invest*. 1986;78:760–770.
36. Kitakaze M, Hori M, Sato H, et al. Endogenous adenosine inhibits platelet aggregation during myocardial ischemia. *Circ Res*. 1991;69:1402–1408.
37. Hausenloy DJ, Yellon DM. New directions for protecting the heart against ischaemia-reperfusion injury: targeting the reperfusion injury salvage kinase (RISK)-pathway. *Cardiovasc Res*. 2004;61:448–460.
38. Trincavelli ML, Tuscano D, Marroni M, et al. Involvement of mitogen protein kinase cascade in agonist-mediated human A_3 adenosine receptor regulation. *Biochim Biophys Acta*. 2002;1591:55–62.
39. Yang XM, Krieg T, Cui L, et al. NECA and bradykinin at reperfusion reduce infarction in rabbit hearts by signaling through PI3K, ERK, and NO. *J Mol Cell Cardiol*. 2004;36:411–421.
40. Boucher M, Pesant S, Falcao S, et al. Post-ischemic cardioprotection by A2A adenosine receptors: dependent of phosphatidylinositol 3-kinase pathway. *J Cardiovasc Pharmacol*. 2004;43:416–422.
41. Kawasaki K, Smith RS Jr, Hsieh CM, et al. Activation of the phosphatidylinositol 3-kinase protein kinase Akt pathway mediates nitric oxide–induced endothelial cell migration and angiogenesis. *Mol Cell Biol*. 2003;23:5726–5737.
42. Richardt G, Waas W, Kranzhofer R, et al. Interaction between the release of adenosine and noradrenaline during sympathetic stimulation: a feed-back mechanism in rat heart. *J Mol Cell Cardiol*. 1989;21:269–277.
43. Buga GM, Griscavage JM, Rogers NE, et al. Negative feedback regulation of endothelial cell function by nitric oxide. *Circ Res*. 1993;73: 808–812.

Am J Physiol Heart Circ Physiol 287: H2670–H2676, 2004
First published July 29, 2004; doi:10.1152/ajpheart.01071.2003

Intravenous administration of mesenchymal stem cells improves cardiac function in rats with acute myocardial infarction through angiogenesis and myogenesis

Noritoshi Nagaya,[1,2] Takafumi Fujii,[3] Takashi Iwase,[1] Hajime Ohgushi,[4] Takefumi Itoh,[1] Masaaki Uematsu,[5] Masakazu Yamagishi,[2] Hidezo Mori,[3] Kenji Kangawa,[6] and Soichiro Kitamura[7]

Departments of [1]Regenerative Medicine and Tissue Engineering, [3]Cardiac Physiology, and [6]Biochemistry, National Cardiovascular Center Research Institute, Osaka 565-8565; Departments of [2]Internal Medicine and [7]Cardiovascular Surgery, National Cardiovascular Center, Osaka; [4]Tissue Engineering Research Center, National Institute of Advanced Industrial Science and Technology, Hyogo; and [5]Cardiovascular Division, Kansai Rosai Hospital, Hyogo 660-8511, Japan

Submitted 10 November 2003; accepted in final form 13 July 2004

Nagaya, Noritoshi, Takafumi Fujii, Takashi Iwase, Hajime Ohgushi, Takefumi Itoh, Masaaki Uematsu, Masakazu Yamagishi, Hidezo Mori, Kenji Kangawa, and Soichiro Kitamura. Intravenous administration of mesenchymal stem cells improves cardiac function in rats with acute myocardial infarction through angiogenesis and myogenesis. *Am J Physiol Heart Circ Physiol* 287: H2670–H2676, 2004. First published July 29, 2004; doi:10.1152/ajpheart.01071.2003.—Mesenchymal stem cells (MSCs) are pluripotent cells that differentiate into a variety of cells, including cardiomyocytes and endothelial cells. However, little information is available regarding the therapeutic potency of systemically delivered MSCs for myocardial infarction. Accordingly, we investigated whether intravenously transplanted MSCs induce angiogenesis and myogenesis and improve cardiac function in rats with acute myocardial infarction. MSCs were isolated from bone marrow aspirates of isogenic adult rats and expanded ex vivo. At 3 h after coronary ligation, 5×10^6 MSCs (MSC group, $n = 12$) or vehicle (control group, $n = 12$) was intravenously administered to Lewis rats. Transplanted MSCs were preferentially attracted to the infarcted, but not the noninfarcted, myocardium. The engrafted MSCs were positive for cardiac markers: desmin, cardiac troponin T, and connexin43. On the other hand, some of the transplanted MSCs were positive for von Willebrand factor and formed vascular structures. Capillary density was markedly increased after MSC transplantation. Cardiac infarct size was significantly smaller in the MSC than in the control group (24 ± 2 vs. 33 ± 2%, $P < 0.05$). MSC transplantation decreased left ventricular end-diastolic pressure and increased left ventricular maximum dP/dt (both $P < 0.05$ vs. control). These results suggest that intravenous administration of MSCs improves cardiac function after acute myocardial infarction through enhancement of angiogenesis and myogenesis in the ischemic myocardium.

left ventricular end-diastolic pressure; cell transplantation; differentiation; homing

INTERRUPTION OF MYOCARDIAL blood flow leads to cardiomyocyte death (20). Although myocyte mitosis and the presence of cardiac precursor cells in adult hearts have recently been reported (6, 17), death of large numbers of cardiomyocytes results in the development of heart failure (16). Thus it would be desirable to induce angiogenesis and myogenesis for the treatment of ischemic heart disease.

Mesenchymal stem cells (MSCs) are pluripotent adult stem cells residing within the bone marrow microenvironment (11, 18). In contrast to their hematopoietic counterparts, MSCs have an adherent nature and are expandable in culture. MSCs can differentiate into not only osteoblasts, chondrocytes, neurons, and skeletal muscle cells but also vascular endothelial cells (19) and cardiomyocytes (23, 24). In vitro, MSCs have the potential to induce a neovascular response in murine Matrigel angiogenesis assay (2). In vivo, local MSC implantation induces therapeutic angiogenesis in a rat model of hindlimb ischemia (1). On the other hand, MSCs directly injected into the infarcted heart have been shown to induce myocardial regeneration and improve cardiac function (21). Stem or progenitor cells have been shown to circulate in peripheral blood and home to ischemic tissues (4). These results raise the possibility that intravenously administered MSCs participate in repair of the ischemic myocardium primarily by angiogenesis, which prevents apoptosis of native cardiomyocytes, and by direct regeneration of lost cardiomyocytes. However, little information is available regarding the therapeutic potential of systemically delivered MSCs for myocardial infarction.

Thus the purpose of this study was to investigate whether *1*) intravenously administered MSCs are able to engraft in the ischemic myocardium, *2*) transplanted MSCs induce angiogenesis and myogenesis after myocardial infarction, and *3*) transplantation of MSCs decreases infarct size and improves cardiac function.

METHODS

Animals. Male Lewis rats ($n = 70$) weighing 220–250 g were used in this study. These isogenic rats ($n = 8$) served as donors and recipients of MSCs to simulate autologous implantation. The Animal Care Committee of the National Cardiovascular Center approved the experimental protocol.

Model of myocardial infarction and cell transplantation. Fifty-one rats underwent ligation of the left coronary artery to produce myocardial infarction, as described previously (15). Briefly, after rats were anesthetized by injection of pentobarbital sodium (30 mg/kg body wt ip), they were artificially ventilated using a volume-regulated respirator. The heart was exposed via a left thoracotomy, and the left coronary artery was ligated 2–3 mm from its origin between the pulmonary artery conus and the left atrium using a 6-0 Prolene suture.

Address for reprint requests and other correspondence: N. Nagaya, Dept. of Regenerative Medicine and Tissue Engineering, National Cardiovascular Center Research Institute, 5-7-1 Fujishirodai, Suita, Osaka 565-8565, Japan (E-mail: nnagaya@ri.ncvc.go.jp).

The costs of publication of this article were defrayed in part by the payment of page charges. The article must therefore be hereby marked "*advertisement*" in accordance with 18 U.S.C. Section 1734 solely to indicate this fact.

At 3 h after coronary ligation, 40 rats survived (78% survival rate): 30 were randomized to receive an intravenous injection of MSCs (MSC group, $n = 14$) or PBS (control group, $n = 16$), and 10 received fluorescence-labeled MSCs for examination of MSC differentiation ($n = 5$) and incorporation ($n = 5$). Eleven rats underwent a sham operation consisting of thoracotomy and cardiac exposure but without coronary artery ligation. At 3 h after coronary ligation, we administered 5×10^6 MSCs/100 μl in PBS or PBS alone through a catheter inserted into the left jugular vein in ~30 s. The subsequent mortality for 4 wk was 25% in the control group and 14% in the MSC group. This protocol resulted in the creation of three groups: normal rats given PBS (sham group, $n = 11$), myocardial infarction rats given PBS (control group, $n = 12$), and myocardial infarction rats given MSCs (MSC group, $n = 12$).

Expansion of bone marrow MSCs. MSC expansion was performed according to previously described methods (18). Briefly, we killed the male Lewis rats and harvested the bone marrow by flushing the cavity of the femurs and tibias with PBS. Bone marrow cells were introduced into 100-mm dishes and cultured in α-MEM supplemented with 10% FBS and antibiotics. A small number of cells developed visible symmetrical colonies by *day 5–7*. Nonadherent hematopoietic cells were removed, and the medium was replaced. The adherent, spindle-shaped MSC population expanded to $>5 \times 10^7$ cells by approximately four to five passages after the cells were first cultured.

Flow cytometry. Adherent cells were analyzed by fluorescence-activated cell sorting (FACS SCAN flow cytometer, Becton Dickinson). Cells were incubated for 30 min at 4°C with the FITC-conjugated mouse monoclonal antibodies against rat CD34 (clone ICO-115, Santa Cruz Biotechnology) and CD45 and CD90 (clones OX-1 and OX-7, respectively, Becton Dickinson). FITC-conjugated hamster anti-rat CD29 monoclonal antibody (clone Ha2/5, Becton Dickinson) and rabbit anti-rat c-Kit polyclonal antibody (clone C-19, Santa Cruz Biotechnology) were used. Isotype-identical antibodies served as controls.

Echocardiographic studies. Echocardiographic studies were performed by an investigator blinded to treatment allocation 4 wk after coronary ligation. Two-dimensional targeted M-mode traces were obtained at the level of the papillary muscles using an echocardiographic system equipped with a 7.5-MHz phased-array transducer (SONOS 5500, Hewlett-Packard, Andover, MA). Anterior and posterior end-diastolic wall thickness and left ventricular (LV) end-diastolic and end-systolic dimensions were measured by the American Society for Echocardiology leading-edge method from at least three consecutive cardiac cycles. LV fractional shortening was calculated as follows: $(LVD_d - LVD_s)/LVD_d \times 100$, where LVD_d is LV diastolic dimension and LVD_s is LV systolic dimension. LV volume and ejection fraction were calculated on the basis of the Teichholtz formula.

Hemodynamic studies. Hemodynamic studies were performed 4 wk after coronary ligation. A 1.5-Fr micromanometer-tipped catheter (Millar Instruments) was inserted in the right carotid artery for measurement of mean arterial pressure. Then the catheter was advanced into the LV for measurement of LV pressure. Hemodynamic variables were measured using a pressure transducer (model P23 ID, Gould) connected to a polygraph. After completion of these measurements, the left and right ventricles were excised and weighed. Infarction size was determined as a percentage of the entire LV area, as reported previously (8). Briefly, incisions were made in the LV, so that the tissue could be pressed flat. The circumference of the entire flat LV and the visualized infarcted area, as judged from the epicardial and endocardial sides, was outlined on a clear plastic sheet. The difference in weight between the two marked areas on the sheet was used to determine infarction size and was expressed as a percentage of LV surface area.

Histological examination. To detect fibrosis in cardiac muscle, the LV myocardium ($n = 5$ each group) was fixed in 10% formalin, cut transversely, embedded in paraffin, and stained with Masson's trichrome. To detect capillary endothelial cells in the peri-infarct area, samples of the harvested muscle ($n = 5$ each) were embedded in OCT compound (Miles Scientific), snap frozen in liquid nitrogen, and cut into transverse sections. Tissue sections were stained for alkaline phosphatase with an indoxyltetrazolium method. The number of capillary vessels was counted in the peri-infarct area using a light microscope at ×200 magnification. The numbers in five high-power fields were averaged and expressed as the number of capillary vessels. These morphometric studies were performed by two examiners who were blinded to treatment.

An additional five rats were used to examine whether transplanted MSCs differentiated into cardiomyocytes or vascular endothelial cells. Suspended MSCs were labeled with fluorescent dyes with a PKH-26 red fluorescent cell linker kit (Sigma Chemical, St. Louis, MO) before implantation, as reported previously (13). Fluorescence-labeled MSCs were intravenously administered 3 h after coronary ligation. This subgroup of rats was killed 4 wk after coronary ligation. After the LV was excised and dissected free, muscle samples were embedded in OCT compound, snap frozen in liquid nitrogen, and cut into sections. Immunofluorescent staining for cardiac and endothelial cell markers was performed using monoclonal mouse antidesmin (Dako), anti-cardiac troponin T (Novo), anticonnexin43 (Sigma Chemical), and polyclonal rabbit anti-von Willebrand factor (Dako). FITC-conjugated IgG antibody (BD Pharmingen and Molecular Probes) was used as a secondary antibody.

At 24 h after intravenous administration of PKH-26-labeled MSCs, cardiac muscle was embedded in OCT compound and snap frozen in liquid nitrogen. Then the cardiac muscle from base to apex was

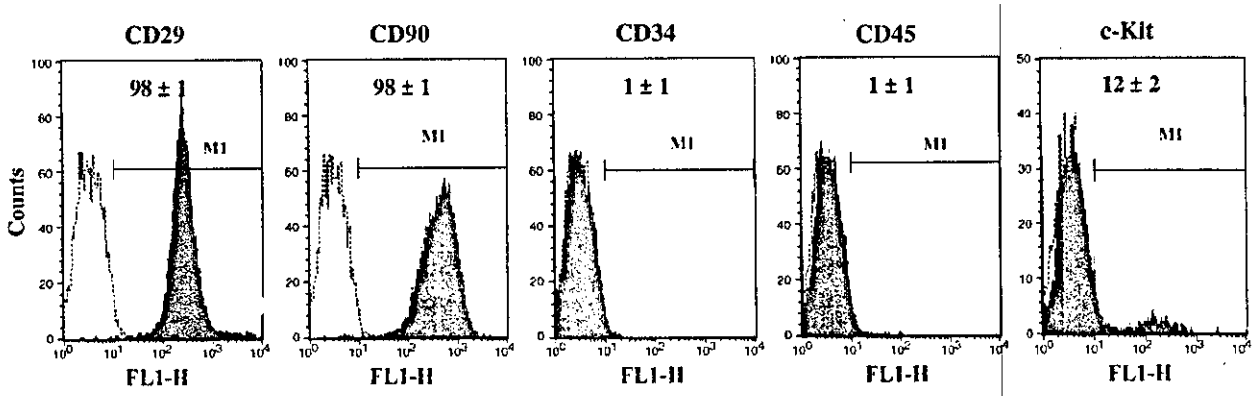

Fig. 1. Flow cytometric analysis of adherent, spindle-shaped mesenchymal stem cell (MSC) population expanded to 4–5 passages. Most of the cells expressed CD29 and CD90 but were negative for CD34 and CD45. Some cells were positive for c-Kit. MI, myocardial infarction.

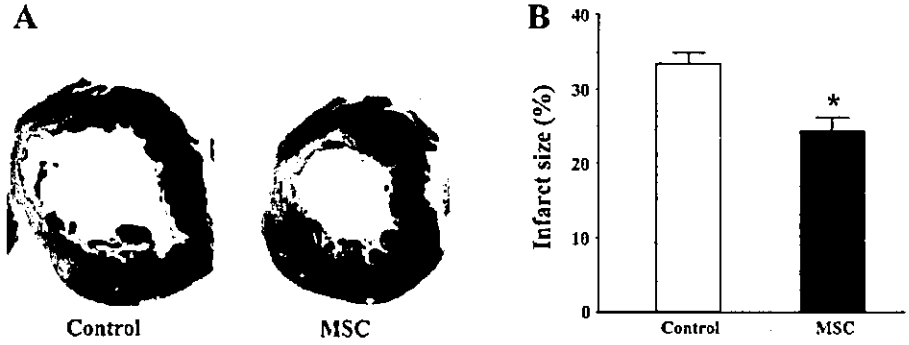

Fig. 2. Effect of MSC transplantation on myocardial infarct size 4 wk after myocardial infarction. *A*: representative Masson's trichrome-stained myocardial sections from control and MSC groups. *B*: quantitative analysis demonstrating that MSC transplantation significantly decreased infarct size. Values are means ± SE. *$P < 0.05$ vs. control.

transversely cut into 5-μm slices for calculation of the numbers of transplanted MSCs in the heart ($n = 5$).

Statistical analysis. Numerical values were expressed as means ± SE unless otherwise indicated. Comparisons of parameters among the three groups were made using one-way analysis of variance (ANOVA) followed by Scheffé's multiple comparison test. Comparisons of parameters between two groups were made by unpaired Student's *t*-test. $P < 0.05$ was considered significant.

RESULTS

Characterization of cultured MSCs. Most of cultured adherent cells expressed CD29 and CD90 (Fig. 1). In contrast, a majority of adherent cells were negative for CD34 and CD45. A small fraction of the adherent cells expressed c-Kit. Thus we confirmed that the major population of adherent cells was MSCs.

Reduction of myocardial infarct size after MSC transplantation. Moderate-to-large infarcts were observed in Masson's trichrome-stained myocardial sections 4 wk after coronary ligation (control group; Fig. 2*A*). However, MSC transplantation markedly decreased the infarct size after myocardial infarction (MSC group). Quantitative analysis also demonstrated that cardiac infarct size was significantly smaller in the MSC than in the control group: 24 ± 2 vs. 33 ± 2% ($n = 12$ each, $P < 0.05$; Fig. 2*B*).

Hemodynamic effects of MSC transplantation. At 4 wk after coronary ligation, hemodynamic studies were performed in the sham ($n = 11$), control ($n = 12$), and MSC ($n = 12$) groups. LV end-diastolic pressure showed a marked elevation in the control group (18 ± 1 mmHg); the elevation was significantly attenuated in the MSC group (13 ± 1 mmHg, $P < 0.05$; Fig. 3*A*). LV maximum dP/d*t* was significantly higher in the MSC than in the control group (Fig. 3*B*). LV minimum dP/d*t* tended to be lower in the MSC than in the control group (Fig. 3*C*). Although mean arterial pressure was significantly lower in the control than in the sham group, no decrease was observed in the MSC group (Table 1). Heart rate did not significantly differ among the three groups.

LV diastolic dimension was significantly smaller in the MSC than in the control group (Table 2). Fractional shortening was significantly greater in the MSC than in the control group (Fig. 3*D*). LV ejection fraction was also higher in the MSC than in

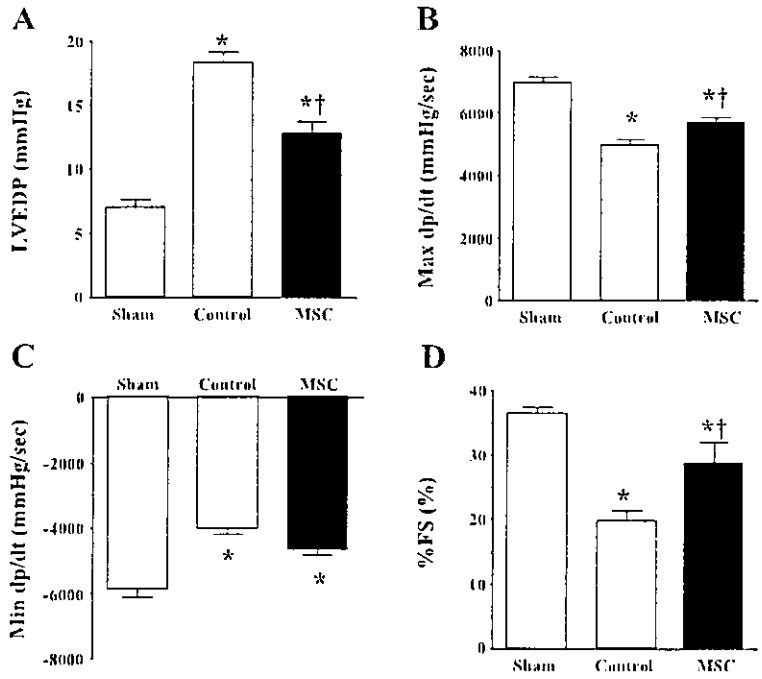

Fig. 3. Effects of MSC transplantation on hemodynamic parameters. LVEDP, LV end-diastolic pressure (*A*); max dP/d*t*, LV maximum dP/d*t* (*B*); Min dP/d*t*, LV minimum dP/d*t* (*C*); %FS, LV fractional shortening (*D*). Values are means ± SE. *$P < 0.05$ vs. sham †$P < 0.05$ vs. control.

Table 1. *Characterization of animals*

	Sham (n = 11)	Control (n = 12)	MSC (n = 12)
Body wt, g	331 ± 4	301 ± 7*	321 ± 7†
LV wt/body wt, g/kg	1.83 ± 0.11	2.22 ± 0.10*	2.17 ± 0.09*
RV wt/body wt, g/kg	0.55 ± 0.02	0.83 ± 0.04*	0.71 ± 0.03*†
Heart rate, beats/min	404 ± 15	428 ± 17	418 ± 15
Mean arterial pressure, mmHg	128 ± 2	113 ± 4*	119 ± 3

Values are means ± SE. Sham, sham-operated rats given vehicle; control, myocardial infarction rats given vehicle; MSC, myocardial infarction rats given mesenchymal stem cells; LV, left ventricle; RV, right ventricle. *P < 0.05 vs. sham. †P < 0.05 vs. control.

Table 2. *Echocardiographic data*

	Sham	Control	MSC
LVD_d, mm	6.3 ± 0.1	8.6 ± 0.2*	7.5 ± 0.3*†
LVD_s, mm	4.0 ± 0.1	6.9 ± 0.3*	5.5 ± 0.5*†
%FS, %	37 ± 1	20 ± 2*	29 ± 3*†
LVEF, %	65 ± 1	39 ± 3*	53 ± 5*†
AWT diastole, mm	1.6 ± 0.1	1.1 ± 0.1*	1.4 ± 0.1†
PWT diastole, mm	1.6 ± 0.1	1.7 ± 0.1	1.7 ± 0.1

Values are means ± SE. LVD_d, LV diastolic dimension; LVD_s, LV systolic dimension; %FS, LV fractional shortening; LVEF, LV ejection fraction; AWT, anterior wall thickness; PWT, posterior wall thickness. *P < 0.05 vs. sham. †P < 0.05 vs. control.

the control group (Table 2). Diastolic anterior wall thickness was significantly attenuated in the MSC group compared with the control group.

Myogenesis and angiogenesis induced by MSCs. Red fluorescence-labeled MSCs were intravenously administered 3 h after coronary ligation (n = 5). Semiquantitative analysis demonstrated that ~3% of the transplanted MSCs were incorporated into the heart 24 h after transplantation. At 4 wk after transplantation (n = 5), MSCs were incorporated predominantly into the border zone of infarcts (Fig. 4), whereas few MSCs were detected in the noninfarcted myocardium. Immunofluorescence analyses demonstrated that the engrafted MSCs were positive for desmin (Fig. 4), cardiac troponin T (Fig. 5*A*), and connexin43 (Fig. 5*B*). These results suggest the ability of MSCs to engraft in the ischemic myocardium and differentiate into cardiomyocytes. On the other hand, some of the transplanted MSCs were positive for von Willebrand factor and formed vascular structures (Fig. 6). Alkaline phosphatase staining of the ischemic myocardium showed marked augmentation of neovascularization in the MSC group (Fig. 7*A*). Quantitative analysis demonstrated that capillary density was significantly higher in the MSC than in the control group (n = 5 each; Fig. 7*B*).

DISCUSSION

In the present study, we demonstrated that intravenously administered MSCs were capable of engraftment in the ischemic myocardium and that the engrafted MSCs differentiated into cardiomyocytes and vascular endothelial cells, resulting in myogenesis and angiogenesis. We also demonstrated that MSC transplantation decreased myocardial infarct size and improved cardiac function after acute myocardial infarction in rats.

Earlier studies showed that MSCs directly injected into the myocardium or those injected into coronary arteries improve cardiac function after myocardial infarction. However, little information is available regarding the therapeutic potential of systemically delivered MSCs for myocardial infarction. This study demonstrated that intravenous administration of MSCs

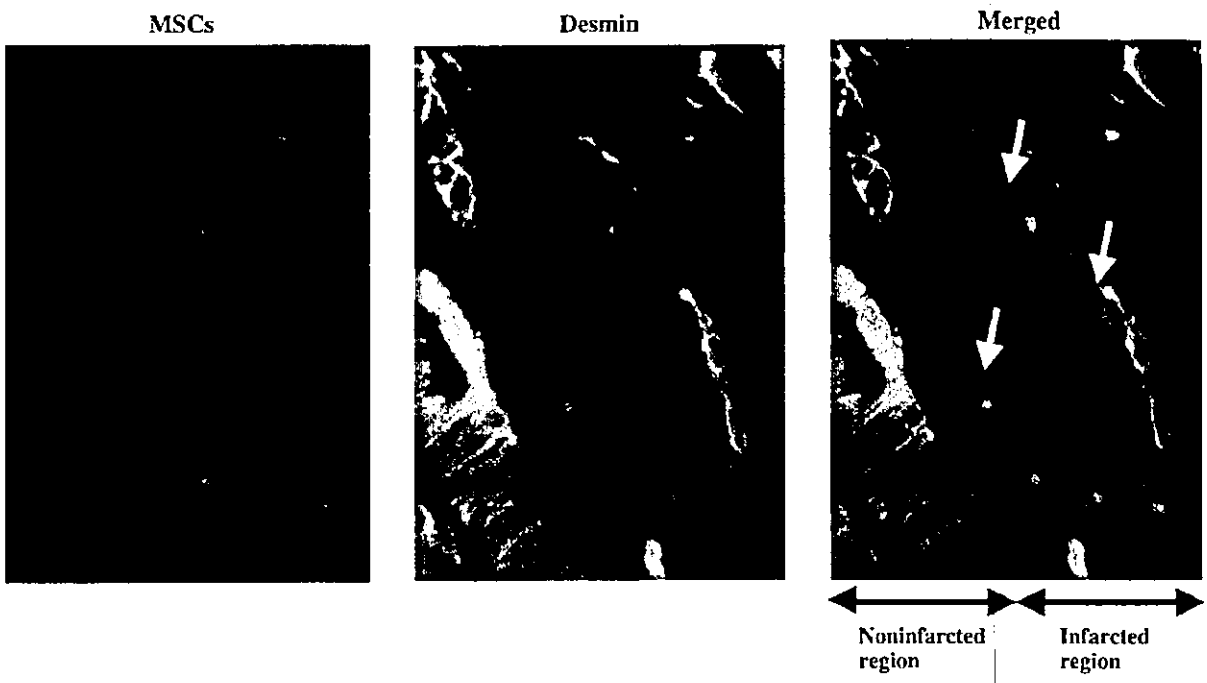

Fig. 4. Distribution of intravenously administered MSCs in myocardium after acute myocardial infarction. Red fluorescence-labeled MSCs were incorporated into ischemic boundary zone of the heart. These cells were positive for desmin (arrows), a cardiac marker. Magnification ×400.

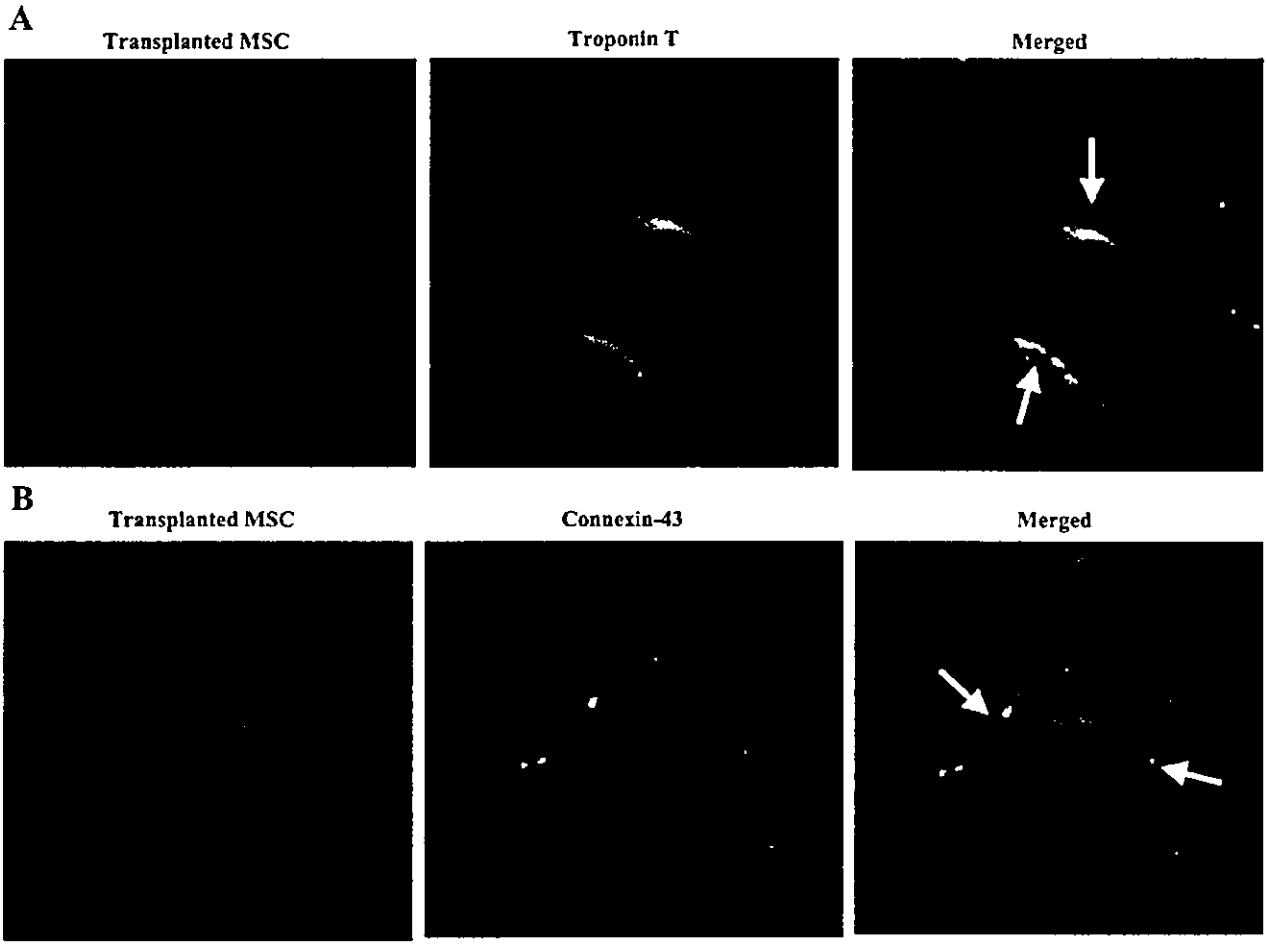

Fig. 5. Differentiation of transplanted MSCs in ischemic myocardium. Engrafted MSCs were positive (arrows) for cardiac troponin T (*A*) and connexin43 (*B*). Magnification ×400.

improves cardiac function after acute myocardial infarction through enhancement of angiogenesis and myogenesis in the ischemic myocardium.

Earlier studies showed that endothelial progenitor cells are mobilized from bone marrow into the peripheral blood in response to tissue ischemia and home to and incorporate into sites of neovascularization (21). Similar to epithelial progenitor cells, in the present study, transplanted MSCs were preferentially attracted to and retained in the border zone of infarcts. This is consistent with recent findings in the ischemic heart (5)

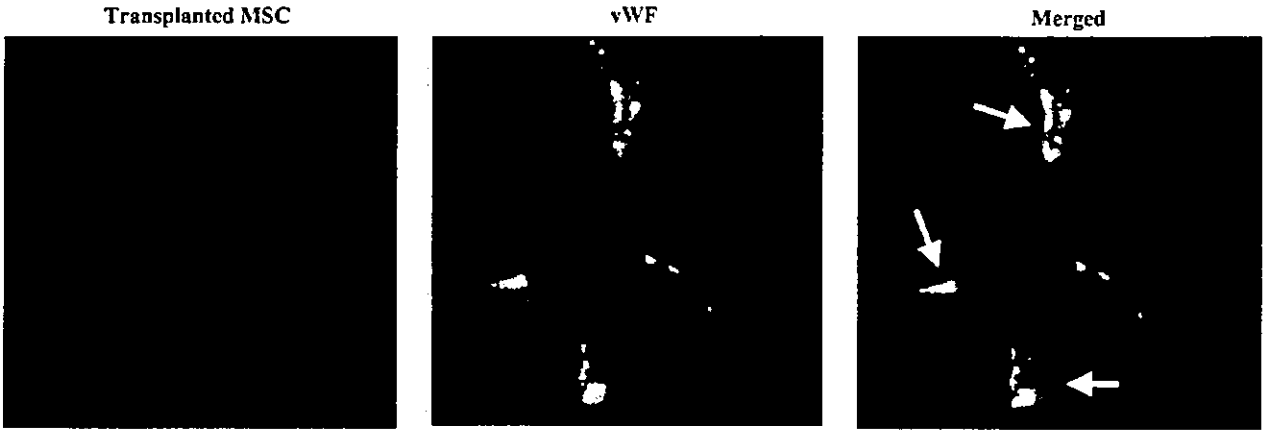

Fig. 6. Transplanted MSCs were positive for von Willebrand factor (vWF) and formed vascular structures. Magnification ×400.

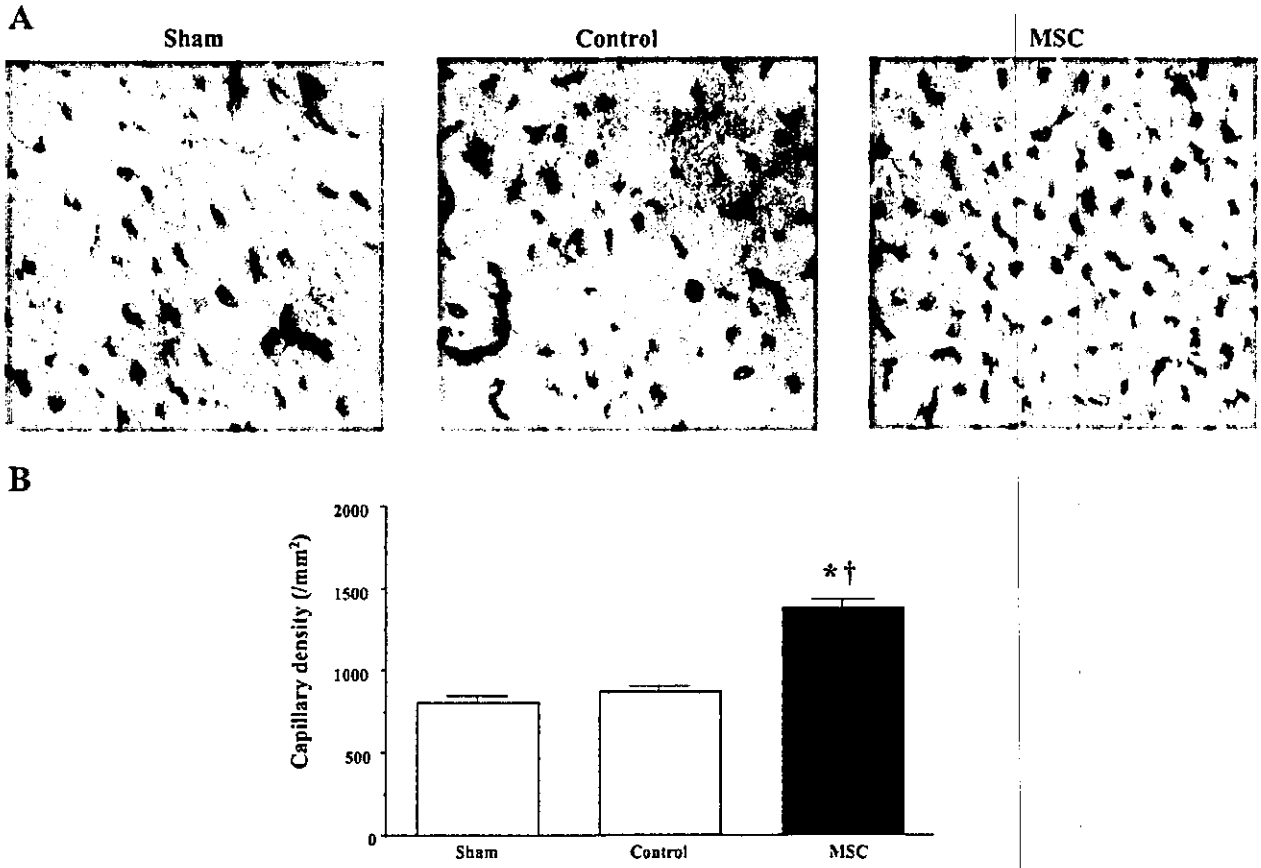

Fig. 7. *A*: representative samples of alkaline phosphatase staining in peri-infarct area. Magnification ×200. *B*: quantitative analysis of capillary density in peri-infarct area. Values are means ± SE. *$P < 0.05$ vs. sham. †$P < 0.05$ vs. control.

or brain (7). Although the underlying mechanisms remain unclear, ischemic tissue may express specific receptors or ligands to facilitate trafficking, adhesion, and infiltration of MSCs to ischemic sites.

In the present study, some of the engrafted MSCs were stained by cardiac proteins such as desmin and cardiac troponin T. Transplanted MSCs also expressed connexin43, a gap junction protein, at contact points with native cardiomyocytes. These results suggest that MSCs differentiated into cardiomyocytes in the ischemic myocardium and formed connections with native cardiomyocytes. In contrast to skeletal myoblasts, which have been used as a tool for myocardial repair, MSCs may have the capacity for electromechanical coupling. Earlier studies demonstrated the importance of the microenvironment for cardiomyogenic differentiation. Possible factors might include direct cell-cell contact (9), electrical and mechanical stimulation (10), and unknown growth factors. On the other hand, recent studies showed that stem cells may fuse with existing native cells (22, 25). Although the mechanisms by which MSCs develop into cardiomyocyte-like cells remain unclear, it is possible that the direct attachment with host cardiomyocytes in the ischemic myocardium contributes to the cardiogenic differentiation of transplanted MSCs. Further studies are necessary to investigate whether engrafted MSCs are actually becoming contractile.

In the present study, some of the transplanted MSCs were positive for an endothelial cell marker and participated in vessel formation. MSC transplantation significantly increased the capillary density in ischemic myocardium. The recently reported phenotypic plasticity of MSCs to transform into endothelial-like cells provides a rationale for their potential role in neovascularization. Hypoxia has been shown to induce MSC migration and capillary-like structure formation by upregulation of membrane type 1 matrix metalloproteinase (3). MSC implantation has been shown to induce therapeutic angiogenesis in a rat model of chronic hindlimb ischemia (1). These findings support the theory that intravenously administered MSCs are able to differentiate into vascular endothelial cells in the ischemic myocardium. Interestingly, MSCs enhance angiogenesis partly by increasing endogenous levels of vascular endothelial growth factor and vascular endothelial growth factor type 2 receptor (7). Together, these findings suggest that MSCs may contribute to neovascularization in the ischemic myocardium not only through their ability to generate capillary-like structures and but also through growth factor-mediated paracrine regulation.

The present study showed that MSC transplantation significantly reduced infarct size and attenuated wall thinning after acute myocardial infarction. Cardiomyocyte apoptosis during ischemia is one of the major contributors to the development of myocardial infarcts (16, 20). It is possible that newly formed vessels after MSC transplantation improve tissue perfusion around the ischemic boundary zone, resulting in functional recovery after acute myocardial infarction. We also demonstrated that transplanted

MSCs differentiated into cardiomyocytes in the ischemic myocardium. These results suggest that the decrease in infarct size and the increase in wall thickness may be attributable not only to MSC-induced neovascularization but also to myocardial regeneration. In the present study, MSC transplantation improved cardiac function after acute myocardial infarction, as indicated by a significant decrease in LV end-diastolic pressure, a tendency for an increase in maximum LV dP/dt, and a decrease in minimum LV dP/dt. Thus MSC-induced angiogenesis and myogenesis and the resultant reduced infarct size may have contributed to the hemodynamic improvement after acute myocardial infarction.

The low percentage of MSC migration to the heart is in agreement with some previous studies (5, 14). The present study also showed that only a small percentage of transplanted MSCs were incorporated into the heart. This may be explained by MSC apoptosis (12), tracking in the lung (5), and a dilution of the fluorescent dyes as the cells reproduce. Nevertheless, when MSCs were intravenously administered in an acute phase of myocardial infarction, MSCs induced angiogenesis and myogenesis and modestly, but significantly, improved cardiac function. Thus systemic delivery of MSCs may be beneficial for the treatment of myocardial infarction.

A limitation of this study is that the cell population may be mixed, rather than limited to MSCs, although cell surface markers of cultured cells were consistent with those of previously reported MSCs (12, 18).

In conclusion, intravenously administered MSCs were preferentially attracted to the infarcted myocardium and differentiated into vascular endothelial cells and cardiomyocytes. MSC transplantation decreased the infarct size and improved cardiac function after acute myocardial infarction through enhancement of angiogenesis and myogenesis. Thus MSC transplantation may be a new therapeutic strategy for the treatment of myocardial infarction.

GRANTS

This work was supported by Ministry of Health, Labour, and Welfare Cardiovascular Disease Research Grant 16C-6, the New Energy and Industrial Technology Development Organization of Japan Industrial Technology Research Grant Program in '03, Health and Labor Sciences Research Grants-genome 005, and Promotion of Fundamental Studies in Health Science of the Organization for Pharmaceutical Safety and Research of Japan.

REFERENCES

1. **Al-Khaldi A, Al-Sabti H, Galipeau J, and Lachapelle K.** Therapeutic angiogenesis using autologous bone marrow stromal cells: improved blood flow in a chronic limb ischemia model. *Ann Thorac Surg* 75: 204–209, 2003.
2. **Al-Khaldi A, Eliopoulos N, Martineau D, Lejeune L, Lachapelle K, and Galipeau J.** Postnatal bone marrow stromal cells elicit a potent VEGF-dependent neoangiogenic response in vivo. *Gene Ther* 10: 621–629, 2003.
3. **Annabi B, Lee YT, Turcotte S, Naud E, Desrosiers RR, Champagne M, Eliopoulos N, Galipeau J, and Beliveau R.** Hypoxia promotes murine bone-marrow-derived stromal cell migration and tube formation. *Stem Cells* 21: 337–347, 2003.
4. **Asahara T, Murohara T, Sullivan A, Silver M, van der Zee R, Li T, Witzenbichler B, Schatteman G, and Isner JM.** Isolation of putative progenitor endothelial cells for angiogenesis. *Science* 275: 964–967, 1997.
5. **Barbash IM, Chouraqui P, Baron J, Feinberg MS, Etzion S, Tessone A, Miller L, Guetta E, Zipori D, Kedes LH, Kloner RA, and Leor J.** Systemic delivery of bone marrow-derived mesenchymal stem cells to the infarcted myocardium: feasibility, cell migration, and body distribution. *Circulation* 108: 863–868, 2003.
6. **Beltrami AP, Urbanek K, Kajstura J, Yan SM, Finato N, Bussani R, Nadal-Ginard B, Silvestri F, Leri A, Beltrami CA, and Anversa P.** Evidence that human cardiac myocytes divide after myocardial infarction. *N Engl J Med* 344: 1750–1757, 2001.
7. **Chen J, Zhang ZG, Li Y, Wang L, Xu YX, Gautam SC, Lu M, Zhu Z, and Chopp M.** Intravenous administration of human bone marrow stromal cells induces angiogenesis in the ischemic boundary zone after stroke in rats. *Circ Res* 92: 692–699, 2003.
8. **Chien YW, Barbee RW, MacPhee AA, Frohlich ED, and Trippodo NC.** Increased ANF secretion after volume expansion is preserved in rats with heart failure. *Am J Physiol Regul Integr Comp Physiol* 254: R185–R191, 1988.
9. **Fukuhara S, Tomita S, Yamashiro S, Morisaki T, Yutani C, Kitamura S, and Nakatani T.** Direct cell-cell interaction of cardiomyocytes is key for bone marrow stromal cells to go into cardiac lineage in vitro. *J Thorac Cardiovasc Surg* 125: 1470–1480, 2003.
10. **Iijima Y, Nagai T, Mizukami M, Matsuura K, Ogura T, Wada H, Toko H, Akazawa H, Takano H, Nakaya H, and Komuro I.** Beating is necessary for transdifferentiation of skeletal muscle-derived cells into cardiomyocytes. *FASEB J* 17: 1361–1363, 2003.
11. **Makino S, Fukuda K, Miyoshi S, Konishi F, Kodama H, Pan J, Sano M, Takahashi T, Hori S, Abe H, Hata J, Umezawa A, and Ogawa S.** Cardiomyocytes can be generated from marrow stromal cells in vitro. *J Clin Invest* 103: 697–705, 1999.
12. **Mangi AA, Noiseux N, Kong D, He H, Rezvani M, Ingwall JS, and Dzau VJ.** Mesenchymal stem cells modified with Akt prevent remodeling and restore performance of infarcted hearts. *Nat Med* 9: 1195–1201, 2003.
13. **Messina LM, Podrazik RM, Whitehill TA, Ekhterae D, Brothers TE, Wilson JM, Burkel WE, and Stanley JC.** Adhesion and incorporation of lacZ-transduced endothelial cells into the intact capillary wall in the rat. *Proc Natl Acad Sci USA* 89: 12018–12022, 1992.
14. **Muller P, Pfeiffer P, Koglin J, Schafers HJ, Seeland U, Janzen I, Urbschat S, and Bohm M.** Cardiomyocytes of noncardiac origin in myocardial biopsies of human transplanted hearts. *Circulation* 106: 31–35, 2002.
15. **Nagaya N, Nishikimi T, Yoshihara F, Horio T, Morimoto A, and Kangawa K.** Cardiac adrenomedullin gene expression and peptide accumulation after acute myocardial infarction in rats. *Am J Physiol Regul Integr Comp Physiol* 278: R1019–R1026, 2000.
16. **Narula J, Haider N, Virmani R, DiSalvo TG, Kolodgie FD, Hajjar RJ, Schmidt U, Semigran MJ, Dec GW, and Khaw BA.** Apoptosis in myocytes in end-stage heart failure. *N Engl J Med* 335: 1182–1189, 1996.
17. **Oh H, Bradfute SB, Gallardo TD, Nakamura T, Gaussin V, Mishina Y, Pocius J, Michael LH, Behringer RR, Garry DJ, Entman ML, and Schneider MD.** Cardiac progenitor cells from adult myocardium: homing, differentiation, and fusion after infarction. *Proc Natl Acad Sci USA* 100: 12313–12318, 2003.
18. **Pittenger MF, Mackay AM, Beck SC, Jaiswal RK, Douglas R, Mosca JD, Moorman MA, Simonetti DW, Craig S, and Marshak DR.** Multilineage potential of adult human mesenchymal stem cells. *Science* 284: 143–147, 1999.
19. **Reyes M, Dudek A, Jahagirdar B, Koodie L, Marker PH, and Verfaillie CM.** Origin of endothelial progenitors in human postnatal bone marrow. *J Clin Invest* 109: 337–346, 2002.
20. **Saraste A, Pulkki K, Kallajoki M, Henriksen K, Parvinen M, and Voipio-Pulkki LM.** Apoptosis in human acute myocardial infarction. *Circulation* 95: 320–323, 1997.
21. **Shake JG, Gruber PJ, Baumgartner WA, Senechal G, Meyers J, Redmond JM, Pittenger MF, and Martin BJ.** Mesenchymal stem cell implantation in a swine myocardial infarct model: engraftment and functional effects. *Ann Thorac Surg* 73: 1919–1925, 2002.
22. **Terada N, Hamazaki T, Oka M, Hoki M, Mastalerz DM, Nakano Y, Meyer EM, Morel L, Petersen BE, and Scott EW.** Bone marrow cells adopt the phenotype of other cells by spontaneous cell fusion. *Nature* 416: 542–545, 2002.
23. **Toma C, Pittenger MF, Cahill KS, Byrne BJ, and Kessler PD.** Human mesenchymal stem cells differentiate to a cardiomyocyte phenotype in the adult murine heart. *Circulation* 105: 93–98, 2002.
24. **Wang JS, Shum-Tim D, Galipeau J, Chedrawy E, Eliopoulos N, and Chiu RC.** Marrow stromal cells for cellular cardiomyoplasty: feasibility and potential clinical advantages. *J Thorac Cardiovasc Surg* 120: 999–1005, 2000.
25. **Ying QL, Nichols J, Evans EP, and Smith AG.** Changing potency by spontaneous fusion. *Nature* 416: 545–548, 2002.

Demonstration of enhanced *K*-edge angiography using a cerium target x-ray generator

Eiichi Sato[a)]
Department of Physics, Iwate Medical University, Morioka 020-0015, Japan

Etsuro Tanaka
Department of Nutritional Science, Faculty of Applied Bio-science, Tokyo University of Agriculture, Setagayaku 156-8502, Japan

Hidezo Mori
Department of Cardiac Physiology, National Cardiovascular Center Research Institute, Osaka 565-8565, Japan

Toshiaki Kawai
Electron Tube Division #2, Hamamatsu Photonics Inc., Iwata-gun 438-0193, Japan

Toshio Ichimaru
Department of Radiological Technology, School of Health Sciences, Hirosaki University, Hirosaki 036-8564, Japan

Shigehiro Sato
Department of Microbiology, School of Medicine, Iwate Medical University, Morioka 020-8505, Japan

Kazuyoshi Takayama
Shock Wave Research Center, Institute of Fluid Science, Tohoku University, Sendai 980-8577, Japan

Hideaki Ido
Department of Applied Physics and Informatics, Faculty of Engineering, Tohoku Gakuin University, Tagajo 985-8537, Japan

(Received 18 May 2004; revised 8 July 2004; accepted for publication 14 August 2004; published 22 October 2004)

The cerium target x-ray generator is useful in order to perform enhanced *K*-edge angiography using a cone beam because *K*-series characteristic x rays from the cerium target are absorbed effectively by iodine-based contrast mediums. The x-ray generator consists of a main controller, a unit with a Cockcroft-Walton circuit and a fixed anode x-ray tube, and a personal computer. The tube is a glass-enclosed diode with a cerium target and a 0.5-mm-thick beryllium window. The maximum tube voltage and current were 65 kV and 0.4 mA, respectively, and the focal-spot sizes were 1.0 $\times$1.3 mm. Cerium $K\alpha$ lines were left using a barium sulfate filter, and the x-ray intensity was 0.48 μC/kg at 1.0 m from the source with a tube voltage of 60 kV, a current of 0.40 mA, and an exposure time of 1.0 s. Angiography was performed with a computed radiography system using iodine-based microspheres. In coronary angiography of nonliving animals, we observed fine blood vessels of approximately 100 μm with high contrasts. © *2004 American Association of Physicists in Medicine.* [DOI: 10.1118/1.1803433]

Key words: x-ray source, x-ray tube, x-ray spectra, attenuation coefficient, angiography

I. INTRODUCTION

Synchrotrons generate monochromatic parallel x-ray beams using single crystals. These beams with photon energies of approximately 35 keV have been employed to perform enhanced *K*-edge angiography,[1–4] since the beams are absorbed effectively by iodine-based contrast mediums. However, it is difficult to increase the irradiation field, due to the parallel beam, and to obtain sufficient machine times for various research projects, including medical applications.

Currently, flash x-ray generators utilize cold-cathode radiation tubes and produce extremely short x-ray pulses of less than 1 μs. So far, several different flash x-ray generators have been developed,[5] and the generators with photon energies of lower than 150 keV[6–11] can be employed to perform biomedical radiography. In order to produce monochromatic x rays, plasma flash x-ray generators are useful, since quite intense and clean characteristic x rays have been produced from weakly ionized linear plasmas of nickel, copper,[12] and molybdenum,[13] while bremsstrahlung rays are hardly detected at all. Using these generators, the characteristic x-ray intensity substantially increased with corresponding increases in the charging voltage.

Since *K*-series characteristic x rays from cerium target are absorbed effectively by iodine-based contrast mediums, a cerium-target x-ray tube is very useful in order to perform high contrast angiography. On the other hand, cerium is a rare earth element and has a high reactivity, and it is difficult to design the target. However, we are very interested in pro-

 0094-2405/2004/31(11)/3017/5/$22.00

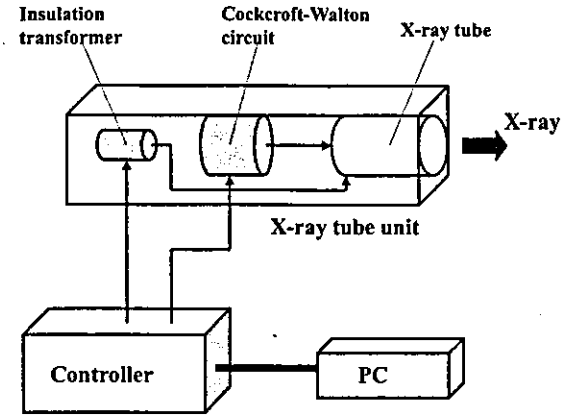

FIG. 1. Block diagram of the compact x-ray generator with a cerium-target radiation tube, which is used specially for *K*-edge angiography using iodine-based contrast mediums.

ducing cerium characteristic x rays to perform cone beam angiography because the irradiation field can be increased easily.

In the present research, we developed a compact x-ray generator with a cerium target tube, and used it to perform a preliminary study on enhanced *K*-edge angiography achieved with cerium $K\alpha$ rays.

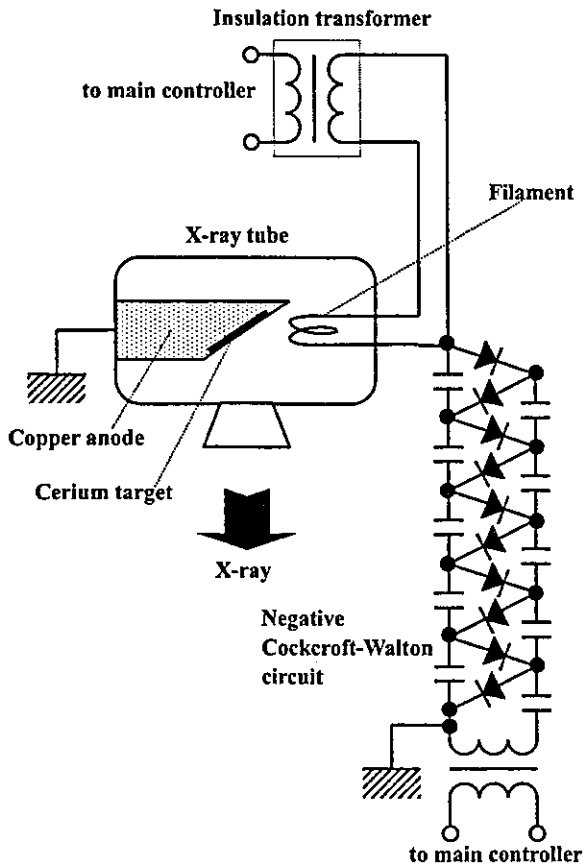

FIG. 2. Main circuit of the x-ray generator.

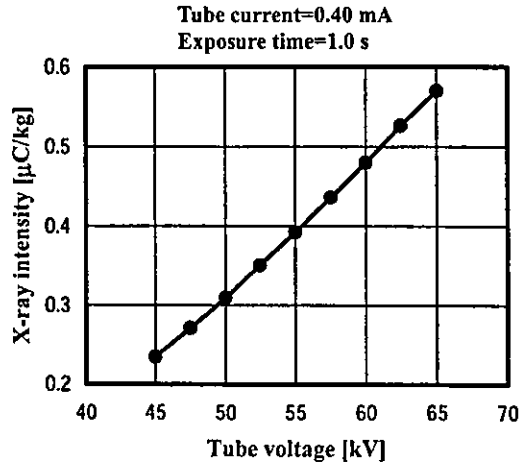

FIG. 3. X-ray intensity measured at 1.0 m from the x-ray source according to changes in the tube voltage.

II. GENERATOR

Figure 1 shows the block diagram of the x-ray generator, which consists of a main controller, an x-ray tube unit with a Cockcroft-Walton circuit, and a cerium-target tube, and a personal computer. The tube voltage, the current, and the exposure time can be controlled by both the controller and the computer. The main circuit for producing x rays is illustrated in Fig. 2, and employed the Cockcroft-Walton circuit in order to decrease the dimensions of the tube unit. In the circuit, the condensers are always in series, and are charged serially. In the x-ray tube, the negative high voltage is applied to the cathode electrode, and the anode (target) is connected to the tube unit case (ground potential) to cool the anode and the target effectively. The filament heating current is supplied by an ac power supply in the controller in conjunction with an insulation transformer which is used for isolation from the high voltage from the Cockcroft-Walton circuit. In this experiment, the tube voltage applied was from 45 to 65 kV, and the tube current was regulated to within 0.40 mA (maximum current) by the filament temperature. The exposure time is controlled in order to obtain optimum x-ray intensity. Monochromatic $K\alpha$ lines were left using a 5-mm-thick barium sulfate filter in which barium sulfate powder was mixed with polymethyl methacrylate (PMMA) resin, since both the bremsstrahlung and the $K\beta$ rays were absorbed effectively by the filter. In designing the filter, the surface density of the barium sulfate powder is important, since the x rays are absorbed effectively by the powder as compared with the PMMA resin. In this case, the density was 7.6 mg/cm^2.

III. CHARACTERISTICS

A. X-ray intensity

X-ray intensity was measured by a Victoreen 660 ionization chamber at 1.0 m from the x-ray source using the filter with an exposure time of 1.0 s (Fig. 3). At a constant tube current of 0.40 mA, the x-ray intensity increased when the tube voltage was increased. In this measurement, the inten-

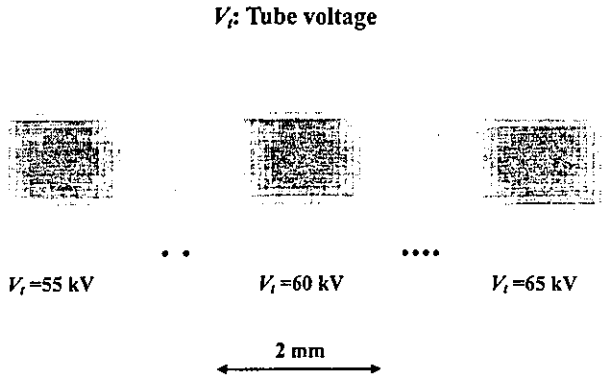

FIG. 4. Effective focal spots with changes in the tube voltage.

sity with a tube voltage of 60 kV and a current of 0.40 mA was 0.48 μC/kg at 1.0 m from the source with errors of less than 0.2%.

B. Focal spot

In order to measure images of the x-ray source after the barium sulfate filtration, we employed a pinhole camera with a hole diameter of 50 μm (magnification ratio of 1:1) in conjunction with a computed radiography (CR) system[14,15] with a sampling pitch of 87.5 μm. When the tube voltage was increased, spot dimensions seldom varied and had values of 1.0×1.3 mm (Fig. 4).

C. X-ray spectra

In order to measure x-ray spectra, we employed a cadmium tellurium detector (CDTE2020X, Hamamatsu Photonics Inc.) (Fig. 5). Compared with a germanium detector, this detector has a lower energy resolution of 1.7 keV. When the tube voltage was increased, the characteristic x-ray intensities of $K\alpha$ lines increased, and both the maximum photon energy and the intensities of bremsstrahlung x rays increased. The barium sulfate filter significantly attenuate the spectra above the barium K-edge energy of 37.399 keV. The areas under the spectral curves correlate closely to the total x-ray intensities shown in Fig. 3.

IV. ANGIOGRAPHY

Figure 6 shows the mass attenuation coefficients of iodine at the selected energies; the coefficient curve is discontinuous at the iodine K edge. The average photon energy of the cerium $K\alpha$ lines is shown just above the iodine K edge. Cerium is a rare earth element and has a high reactivity; however, the average photon energy of $K\alpha$ lines is 34.566 keV, and iodine contrast mediums with a K-absorption edge of 33.155 keV absorb the lines easily. Therefore, blood vessels were observed with high contrasts. Subsequently, in angiography testing, we usually employ nonliving animal phantoms using microspheres.

The angiography was performed by the CR system (Konica Regius 150) using the filter, and the distance (between the x-ray source and the imaging plate) was 1.5 m.

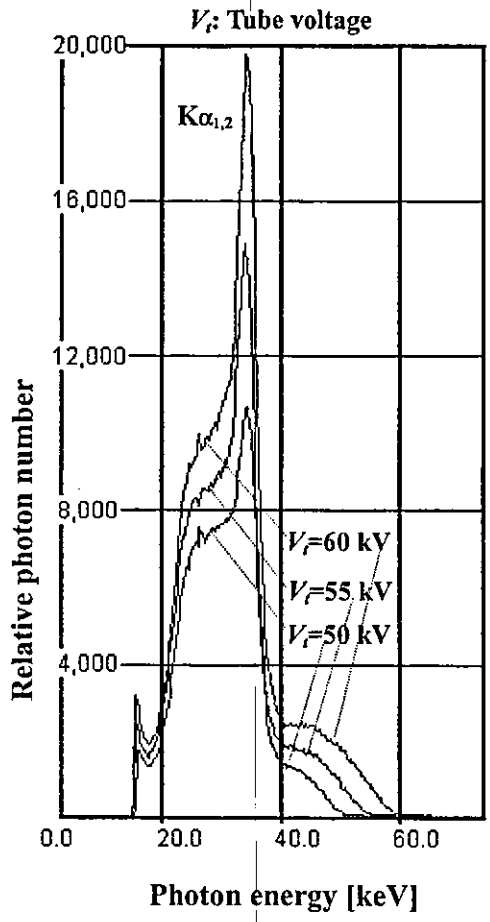

FIG. 5. X-ray spectra measured by a cadmium tellurium detector with changes in the tube voltage.

First, rough measurements of image resolution were made using wires. Figure 7 shows radiograms of tungsten wires in a rod made of PMMA with a tube voltage of 60 kV. Although the image contrast decreased somewhat with decreases in the wire diameter, due to blurring of the image caused by the sampling pitch of 87.5 μm, a 50-μm-diameter wire could be observed.

Angiograms of rabbit hearts are shown in Fig. 8. These two images were obtained using iodine and cerium micro-

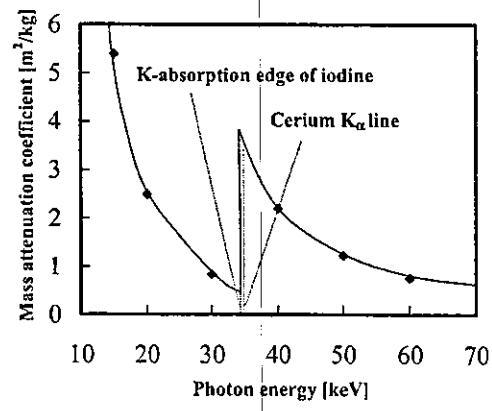

FIG. 6. Mass attenuation coefficients of iodine, and the average photon energy of the cerium $K\alpha$ lines is shown just above the iodine K edge.

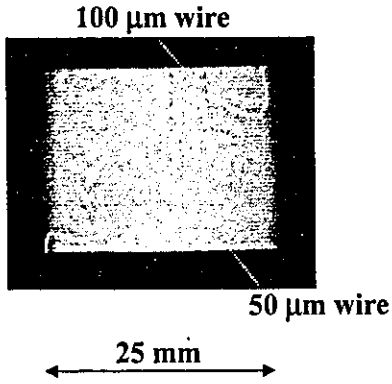

FIG. 7. Radiograms of tungsten wires in a PMMA rod with a tube voltage of 60 kV.

spheres of 15 μm in diameter at a tube voltage of 60 kV. The iodine spheres contained 37% iodine by weight, and the cerium spheres contained 18% cerium by weight. The concentration of spheres in the blood varies with the filling rate, and the estimated densities of the iodine and the cerium of blood are less than 0.44 and 0.17 g/cm^3, respectively. In the case where the cerium spheres were employed, the coronary arteries were barely visible. Figure 9(a) shows an angiogram of a larger dog heart using the cerium target at a tube voltage of 60 kV using iodine spheres. For comparison, we performed angiography with a tungsten x-ray tube at a tube voltage of 60 kV [Fig. 9(b)].

If we assume that the filling rate of the iodine microspheres in a blood vessel is constant, the image contrast of the blood is in inverse proportion to the vessel diameter. Next, the density ratios (maximum density divided by minimum density) obtained by the cerium and tungsten tubes were 4.3 and 2.7, respectively. In angiography using the tungsten target, blood vessels of approximately 100 μm were hardly observed at all.

V. DISCUSSION

In summary, we developed a x-ray generator with a cerium-target tube and succeeded in producing cerium $K\alpha$ lines, which can be absorbed easily by iodine-based contrast mediums. Both the characteristic and bremsstrahlung x-ray

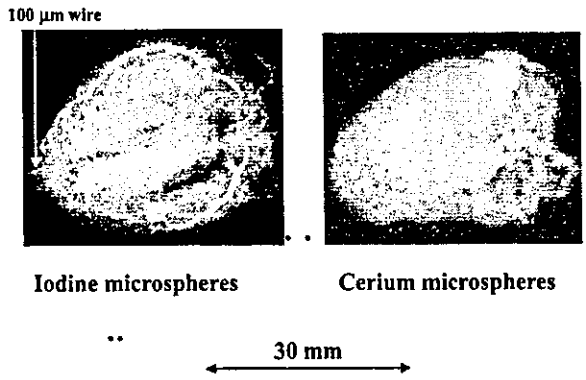

FIG. 8. Angiograms of extracted rabbit hearts using iodine and cerium microspheres with a tube voltage of 60 kV.

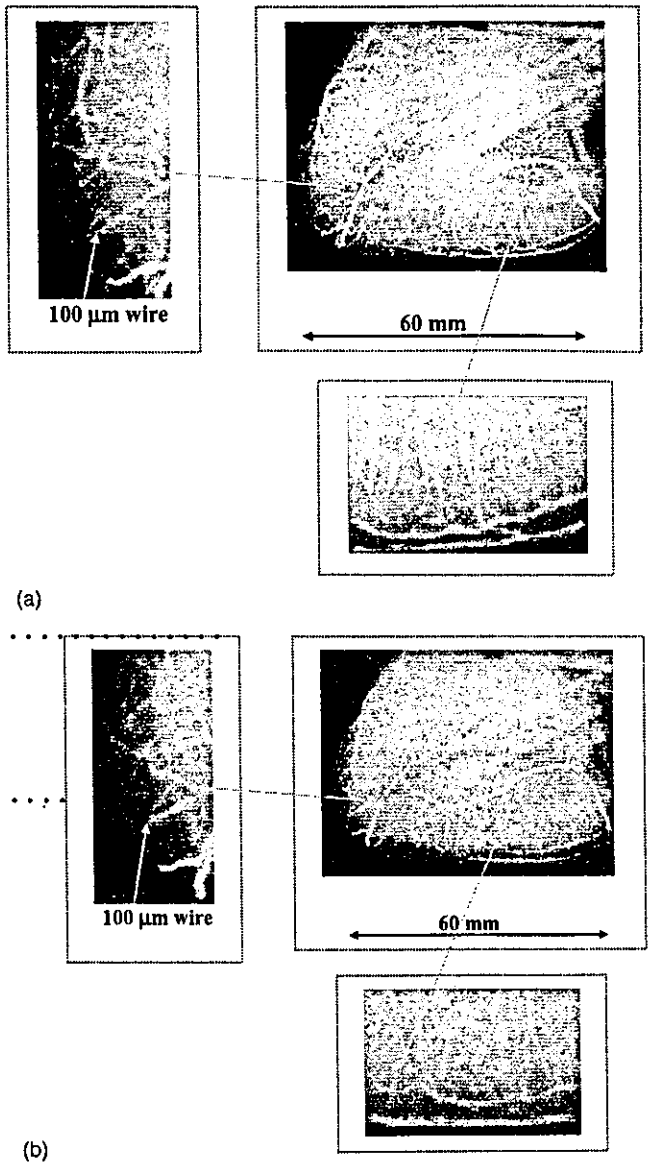

FIG. 9. Angiograms of an extracted dog heart achieved with (a) cerium and (b) tungsten target x-ray tubes using iodine microspheres with a tube voltage of 60 kV.

intensities increased with increases in the tube voltage, and $K\beta$ lines were absorbed effectively by the barium sulfate filter. The x-ray intensity was limited because the thermal contact between the target and the anode was not good. However, the intensity can be increased by welding the target or using a cerium-alloy target.

In this preliminary experiment, although the maximum tube voltage and current were 65 kV and 0.40 mA, respectively, the voltage and current could be increased. Subsequently, the generator produced maximum number of characteristic photons was approximately 3×10^7 photons/cm^2 s at 1.0 m from the source, and the photon count rate can be increased easily by improving the target.

Since the sampling pitch of the CR system is 87.5 μm, we obtained resolutions of approximately 100 μm, and high-contrast blood vessels could be observed using a CR system. In order to observe fine blood vessels of less than 100 μm,

the image resolution of the CR system should be improved as much as possible, and a flat panel system is useful to observe blood flows for cases of cardiovascular disease.

ACKNOWLEDGMENTS

This work was supported by Grants-in-Aid for Scientific Research and Advanced Medical Scientific Research from MECSST (13470154, 13877114, and 16591222), Grants from Keiryo Research Foundation, JST (Test of Fostering Potential), NEDO, and MHLW (HLSRG, RAMT-nano-001, RHGTEFB-genome-005, and RGCD13C-1).

[a]Author to whom correspondence should be addressed. Department of Physics, Iwate Medical University, 3-16-1 Honchodori, Morioka 020-0015, Japan; electronic mail: dresato@iwate-med.ac.jp

[1]A. Akisada, M. Ando, K. Hyodo, S. Hasegawa, K. Konishi, K. Nishimura, A. Maruhashi, F. Toyofuku, A. Suwa, and K. Kohra, "An attempt at coronary angiography with a large size monochromatic SR beam," Nucl. Instrum. Methods Phys. Res. A **246**, 713–718 (1986).

[2]A. C. Thompson, H. D. Zeman, G. S. Brown, J. Morrison, P. Reiser, V. Padmanabahn, L. Ong, S. Green, J. Giacomini, H. Gordon, and E. Rubenstein, "First operation of the medical research facility at the NSLS for coronary angiography," Rev. Sci. Instrum. **63**, 625–628 (1992).

[3]H. Mori, K. Hyodo, E. Tanaka, M. U. Mohammed, A. Yamakawa, Y. Shinozaki, H. Nakazawa, Y. Tanaka, T. Sekka, Y. Iwata, S. Honda, K. Umetani, H. Ueki, T. Yokoyama, K. Tanioka, M. Kubota, H. Hosaka, N. Ishizawa, and M. Ando, "Small-vessel radiography in situ with monochromatic synchrotoron radiation," Radiology **201**, 173–177 (1996).

[4]K. Hyodo, M. Ando, Y. Oku, S. Yamamoto, T. Takeda, Y. Itai, S. Ohtsuka, Y. Sugishita, and J. Tada, "Development of a two-dimensional imaging system for clinical applications of intravenous coronary angiography using intense synchrotron radiation produced by a multipole wiggler," J. Synchrotron Radiat. **5**, 1123–1126 (1998).

[5]R. Germer, "X-ray flash techniques," J. Phys. E **12**, 336–350 (1979).

[6]E. Sato, H. Isobe, and F. Hoshino, "High intensity flash x-ray apparatus for biomedical radiography," Rev. Sci. Instrum. **57**, 1399–1408 (1986).

[7]E. Sato, S. Kimura, S. Kawasaki, H. Isobe, K. Takahashi, Y. Tamakawa, and T. Yanagisawa, "Repetitive flash x-ray generator utilizing a simple diode with a new type of energy-selective function," Rev. Sci. Instrum. **61**, 2343–2348 (1990).

[8]A. Shikoda, E. Sato, M. Sagae, T. Oizumi, Y. Tamakawa, and T. Yanagisawa, "Repetitive flash x-ray generator having a high-durability diode driven by a two-cable-type line pulser," Rev. Sci. Instrum. **65**, 850–856 (1994).

[9]E. Sato, K. Takahashi, M. Sagae, S. Kimura, T. Oizumi, Y. Hayasi, Y. Tamakawa, and T. Yanagisawa, "Sub-kilohertz flash x-ray generator utilizing a glass-enclosed cold-cathode triode," Med. Biol. Eng. Comput. **32**, 289–294 (1994).

[10]K. Takahashi, E. Sato, M. Sagae, T. Oizumi, Y. Tamakawa, and T. Yanagisawa, "Fundamental study on a long-duration flash x-ray generator with a surface-discharge triode," Jpn. J. Appl. Phys., Part 1 **33**, 4146–4151 (1994).

[11]E. Sato, M. Sagae, K. Takahashi, A. Shikoda, T. Oizumi, Y. Hayasi, Y. Tamakawa, and T. Yanagisawa, "10 kHz microsecond pulsed x-ray generator utilizing a hot-cathode triode with variable durations for biomedical radiography," Med. Biol. Eng. Comput. **32**, 295–301 (1994).

[12]E. Sato, Y. Hayasi, R. Germer, E. Tanaka, H. Mori, T. Kawai, T. Ichimaru, K. Takayama, and H. Ido, "Quasi-monochromatic flash x-ray generator utilizing weakly ionized linear copper plasma," Rev. Sci. Instrum. **74**, 5236–5240 (2003).

[13]E. Sato, Y. Hayasi, R. Germer, E. Tanaka, H. Mori, T. Kawai, H. Obara, T. Ichimaru, K. Takayama, and H. Ido, "Irradiation of intense characteristic x-rays from weakly ionized linear molybdenum plasma," Jpn. J. Med. Phys. **23**, 123–131 (2003).

[14]M. Sonoda, M. Takano, J. Miyahara, and H. Kato, "Computed radiography utilizing scanning laser stimulated luminescence," Radiology **148**, 833–838 (1983).

[15]E. Sato, K. Sato, and Y. Tamakawa, "Film-less computed radiography system for high-speed imaging," Ann. Rep. Iwate Med. Univ. Sch. Lib. Arts and Sci. **35**, 13–23 (2000).

生体物理刺激と生体反応

External Physical Stimulation and its Reaction on Human Body

監　修

大森 豊明：OHT技術士事務所 所長

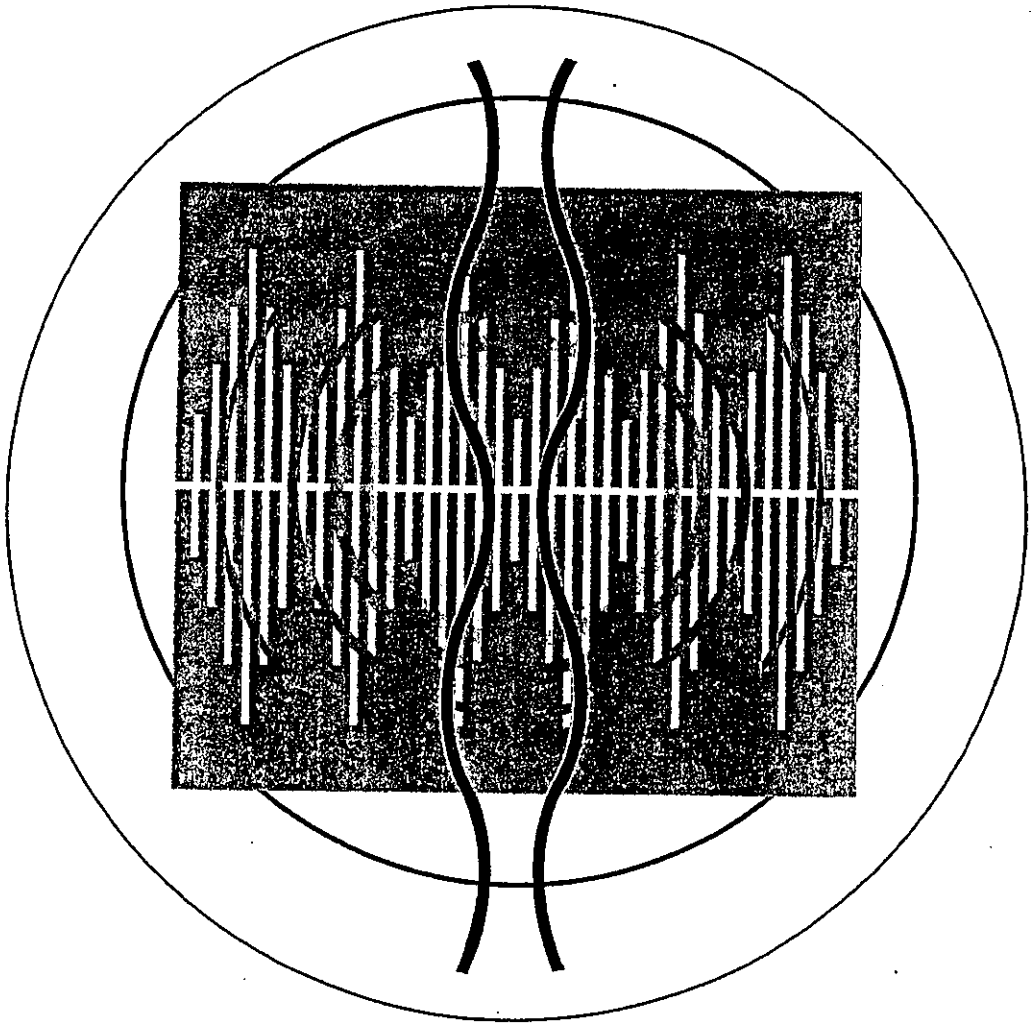

フジ・テクノシステム

第7章

メカニカルストレスに対する細胞応答の分子機構

まえがき

バイオメカニクスは，生体の機能および構造を解析し，その結果を医学，生物学，工学などに応用する新しい研究分野である。バイオメカニクスの領域は広範であるが，本書のテーマである「生体物理刺激と生体反応」をかんがみて分子レベルでの「機械的刺激(メカニカルストレス)に対する細胞応答の分子機構」について紹介する。

近年，分子生物学の進展が著しく，分子レベルでの細胞内の動態の解明がいちだんと進んでいる。メカニカルストレスに対する細胞応答の機序の理解も進みつつある。過剰なメカニカルストレス，あるいは適切な細胞応答能の破綻はさまざまな疾患を引き起こすことを考慮すれば，この分野の研究はそれらの疾患に対する治療法の確立には必須である。また，いうまでもないが分子レベルでの細胞応答の理解が進んだのは，生体組織の力学的性質の理解と，生体に加わる負荷の計測法の開発が進展したからにほかならない。

本章においては，メカニカルストレスに対する生体の反応において，その受容体，シグナル伝達系などについて述べる。

第1節　バイオメカニクスとは

バイオメカニクス(biomechanics)とは生体の機能および構造を力学的に解析し，得られた結果を応用する研究分野である。ヨーロッパにおいて，生体の運動に関する研究を中心としてバイオメカニクスの研究が行われてきたようであるが，1970年前後からアメリカにおいてY. C. Fung教授の指導によってバイオメカニクスは大きな発展を遂げた[1]。現在ではバイオメカニクスの領域を扱う学会も設立され，研究も幅広く行われている。

生体は細胞，組織，個体レベルで内的・外的に常に力学的負荷を受け，生体の機能は常にその影響下で働いている。さらに力学的刺激の変化に鋭敏に反応して，その構造と機能を適応的に変化させることで恒常性を維持している。そのため，力学的刺激に対する生体反応のメカニズムの解析は，生体を理解するうえで非常に重要である。

バイオメカニクスはさまざまに定義されているが，林は「生命体組織全般の構造と機能を力学的観点からとらえて，生体の分子，細胞，組織，器官，あるいはからだ全体のはたらきと生体総合性を解明するとともに，得られた知見を医学における診断，治療，予防はもとより産業上や社会的な諸問題の解決などに応用することを目指す学問・研究領域」[2]と定義している。

力学的解析は現代社会の工業分野の中で重要ではあるが，生物以外の無機物質の解析が中心であった。それは生体についての力学的解析は生体の構造，力学特性が人工物と比較して非常に複雑かつ未知であり，人工物ほどの強靱さがないなどの理由で困難であったなどの理由からである。

バイオメカニクスは，医学的診断・治療法開発や人工臓器開発などを行ううえで非常に重要である。また，生体の構造は進化の過程において最適化が進み完成度がきわめて高いため，その構造原理の理解と応用は工学的技術の開発においても有益性がきわめて高いと考えられる。近年，ナノテクノロジーの発達が著しく，より精密な物質の加工技術が進展していくため，生体を参考とした応用技術の開発はさらに加速していくと予想される。

以上のような理由から，バイオメカニクスの研究の重要性は，今後ますます高くなると考えられる。

バイオメカニクスの分野は広範囲であるが，林は

以下のように大別している[3~6]。

1）生体の構成素材，組織，器官の構造と機能を対象とする分野

2）生体各部やからだ全体の力学的仕組みを対象とする分野

3）ヒトの運動，動作などを対象とする分野

本章においては，1)の分野を取り上げる。さらに，1)の領域としては，①生体を構成する物質，組織，器官の構造および形態，機能，反応などを解析する基礎バイオメカニクス，②人工臓器の開発，治療法の開発などを行う医学的応用，③生体を模倣した材料や設計法の開発などを行う工学応用の3つの応用分野があるとされる[3]。

本章においては，基礎バイオメカニクスのうちとくに機械的負荷（メカニカルストレス）を受けた細胞が，その刺激に対して応答する機序について述べる。メカニカルストレスに対する，細胞応答の作用機構の分子レベルでの解析は，過剰なメカニカルストレスにより引き起こされる疾患の治療法の開発にもつながる重要な研究分野である。

メカニカルストレスを受けた細胞が，その刺激に対して応答する機序はいまだ完全な理解は得られていないため，今後，進展が期待される重要な研究分野である。ここでは主に細胞がメカニカルストレスを受けた際の，その刺激を感知する受容体，受容体をコードする遺伝子，シグナル伝達系などについて複数の知見をまとめて紹介する。

第2節　生体組織の力学的解析と細胞応答の基本概念

1．生体組織の性質

生体組織はさまざまな特徴をもつ有機物質から構成されるため，従来の力学的解析の対象であった無機的な物質とは力学的性質が著しく異なり，新たな解析法を導入する必要があった。

生体の各組織はその構造と物質の組成が異なるため，各組織それぞれの特徴を理解したうえで解析を行う必要があった。さらに，組織そのものの性質のみならず，循環器などの比較的能動的に働く器官においては，血液の流れの性質など流体力学などを導入する必要もあり，生体組織の力学的性質および計測法は非常に複雑である。

1970年前後から，その性質と構成法則の研究により生体組織の力学的特徴の理解が進み，その計測法が開発されたことが背景にある。本章においては生体組織の力学的性質については解説しないが，より詳細な情報を必要とされる方は他の文献を参照されたい。

2．応　力

通常，生体組織は連続体として考えられ，ほとんどの生体組織の運動は連続体の運動として観察される。その解析には物体の運動と変形力の伝達の理解が不可欠であり，そのために連続体力学が導入される。ここでは連続体力学について詳しくは述べないが，生体組織の強度を比較する際の個体による大きさの違いおよび試験方法による違いなどの問題点を解決するために，連続体力学の中の単位面積当たりにかかる力を示す応力（ストレス）が用いられる[7]。

3．メカニカルストレスに対する細胞応答の概念

生体は常に種々の負荷の影響下にあり，その負荷に適応するように構築されている。さらに，その負荷の変化に対応して，生体組織は構造と機能を敏感かつ的確に適応させ，組織の再構築を行って恒常性を維持することが知られている。たとえば，血流と血圧の変化に応答して血管や心臓が再構築を行うことが知られている[8]。

メカニカルストレスは細胞膜に存在する受容体により感知され，主にリン酸化の細胞内シグナルに変換されて，最終的に遺伝子発現を促すことで細胞機能を発揮する。細胞膜上の受容体は刺激を受ける細胞とメカニカルストレスの種類によって異なるが，現在は細胞膜に存在するインテグリンなどの接着分子と，伸展刺激活性化チャネルなどが細胞膜の伸展刺激を感知すると考えられている。

なお，リン酸化によるシグナル伝達においてタンパク質のリン酸化を行うのは，キナーゼ(kinase)と呼ばれるタンパク質をリン酸化する酵素である。キナーゼには，タンパク質を構成するアミノ酸のセ

リン/スレオニンをリン酸化するセリン/スレオニンキナーゼと，チロシンをリン酸化するチロシンキナーゼが存在する。細胞内情報伝達系は，タンパク質が段階的にリン酸化・脱リン酸化されるカスケードシステムである。

第3節　細胞単位の形態変化およびイオンチャネル

1. 血管内皮細胞におけるメカニカルストレスの感知と形態形成

生体組織はメカニカルストレスに応じて，組織の再構築を行う。その例としては，血管に加わる応力の変化に対応して血管壁が厚くなる現象や，心負荷によって心肥大が発生する現象などが知られている[5]。これらの現象は，生体組織が細胞単位で形態を変化させる機能が基礎となって成り立っている。以下に，細胞の形態を決定する機構として明らかになっている知見について述べる。

接着細胞においては，細胞と基質の間に存在する細胞接着斑の中に存在するインテグリンの分布が，細胞の形を決定していると考えられている。さらに，接着斑に存在する他のタンパク質およびアクチン線維が，インテグリンの分布を決定すると推定されているが，その仕組みはいまだ不明である[6]。

細胞にメカニカルストレスがかかると細胞膜が変形することから，刺激を感知する受容体が存在し，受容体が感知した刺激を細胞内シグナルに変換した結果，細胞膜の変形が起こると考えられる。膜張力を感知する伸展活性化チャネル(stretch-activated channel；SA チャネル)と呼ばれる受容体が多くの細胞に存在することが判明している[6,9]。

SA チャネルの中でも，Ca^{2+} および Na^{+} を透過させる陽イオン選択型チャネルが重要である。細胞の形態が変化する際に細胞膜に作用した張力を SA チャネルが感知して，細胞の形態の変化を Ca^{2+} の透過という生化学的シグナルに変換して細胞内部に伝達すると推定されている。しかしながら，SA チャネルが膜張力の情報を，細胞の形態変化という異なる情報に変換する機序は明らかとなっていない[6]。

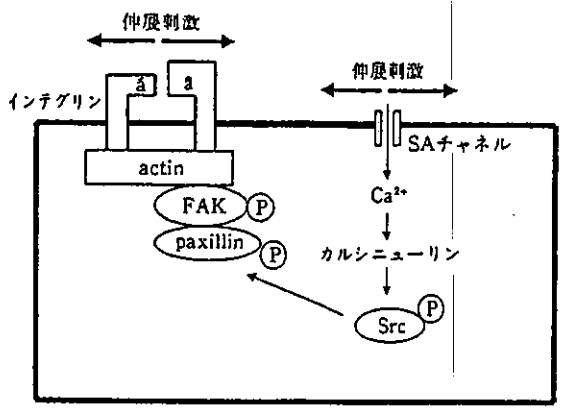

図1　内皮細胞における伸展刺激による細胞内情報伝達機構
伸展刺激はインテグリンを介して細胞膜の伸展と SA チャネルの活性化を誘導する．インテグリンと SA チャネルの2つのシグナル伝達系は接着斑で統合される．(曽我部正博，他：医学のあゆみ，Vol. 192, No. 13, pp. 1201-1205, 図2，2000 を改変)

血管内皮細胞は血管の内側に存在する細胞であり，常に血流と血圧にさらされている。血管の拡張と収縮は，血管の方向に垂直な伸展刺激を血管内皮細胞に作用させる。その結果，細胞の形態は紡錘形となり，さらに多数の細胞がその長軸を血管と平行させて整列する。一定方向の血流が存在しない状態では，血管内皮細胞は定まった形態と配列を構築することはない[8]。その伸展刺激を感知するシグナル伝達機構は，曽我部らは，以下のようなものであると推定している(図1)[8]。

> 周期伸展刺激 → SA チャネル活性化 → 細胞内 Ca^{2+} 濃度の上昇 → カルシニューリンの活性化 → Src キナーゼ活性化 → 接着斑タンパク質(FAX，paxillin など)のチロシンリン酸化 → 細胞骨格と接着斑の再編成 → 形態変化

血管内皮細胞は，伸展刺激を感知するとその伸展方向と垂直の方向に伸長するが，その詳細なメカニズムは不明である。曽我部らは，SA チャネルを介するシグナル伝達系とインテグリン/細胞骨格系を介するシグナル伝達系が接着斑において協調して形態の変化を誘導すると予想している[8]。

2. 伸展活性化 Ca^{2+} 透過チャネル Mid 1 の遺伝子

SA チャネルには，Ca^{2+} などの陽イオンを透過させるタイプと陰イオンを透過させるタイプがある。SA チャネルの活動により，陽イオンおよび陰イオ

ンシグナルの発生と膜の脱分極が起こると推定される。SAチャネルが，広範な細胞に存在することが報告されてきた[8]。真核生物においてはSAチャネルの遺伝子およびタンパク質も特定されていなかった。しかしながら近年，真核生物では初めて出芽酵母のSAチャネル(Ca^{2+}透過性チャネル)の遺伝子としてMID1遺伝子が特定された。

分化した出芽酵母には，Ca^{2+}を細胞内に流入させることができずに死滅する突然変異株，mid1変異株が存在する[10]。MID1遺伝子の導入によってmid1変異株は致死性を失う。すなわち，Ca^{2+}の流入に関与する遺伝子としてMID1遺伝子が特定された[11]。

飯田ら[11]によるとMid1チャネルの構造は，548のアミノ酸残基から構成され，4つの疎水性領域を有し，その1つは形質膜に移行するためのシグナルペプチドであると推定される。Mid1はC末端にジンクフィンガーモチーフ類似の領域を有し，また*N*-グリコシレーション部位が16ヵ所存在する。Mid1はそのアミノ酸配列から，同様の構造を有する4つのユニットから構成され，Ca^{2+}が透過するための通路を構築すると推定されている。Mid1チャネルは，1価の陽イオンを透過させるが，陰イオンは透過させない。さらに他の陽イオンよりもCa^{2+}を透過させる。

さらに，飯田らはSAチャネルの開口は細胞外からの機械的刺激によるばかりではなく，細胞活動自体によっても起こりうることを明らかにした。出芽酵母において，Mid1チャネルは細胞外部からの刺激ではなく，細胞分化に伴う細胞の伸長により開口する。この伸長は形質膜の伸展を引き起こし，その結果，Mid1チャネルを開口させると考えられる。哺乳類細胞においても，形質膜の伸長を伴う複数の活動でCa^{2+}のシグナルが確認されているが，この現象に関わるチャネルは特定されていない[11]。

真核生物からSAチャネル遺伝子が特定され，さらにヒトゲノムの解読がほぼ終了しつつある現在では，ヒトのSAチャネル遺伝子の発見が期待される。

3. 伸展感受性Cl-チャネル

ほとんどのSAチャネルは，Na^+やK^+などの陽イオンが非特異的に透過する。しかしながら，心筋細胞に存在する伸展感受性陰イオン(Cl)チャネルは，Clイオンなどの陰イオンも透過することができる[12]。細胞膜の伸展および細胞膨大により引き起こされる陰イオン電流は，伸展感受性Clチャネルを活性化して，Clイオンなどの陰イオンのみを透過させる。荻原らは，浸透圧が変化して細胞の容積が膨張した場合に，伸展感受性Clチャネルは細胞内の水分を排出し，細胞の容積の増加を抑制する役割があると考えている[12-14]。伸展感受性Clチャネルは，12回の膜貫通領域を有するClC3タンパクが中心となって構成すると考えられている[14]。

第4節 循環器におけるメカニカルストレスに対する細胞応答

細胞はメカニカルストレスにさらされるとその形態を変化させる。この性質に基づいて，血管や心臓の構造の再構築や骨格筋の伸長が行われる[8]。

臨床医学において代表的な分野としては循環器領域があげられる。心肥大は心室にかかる圧負荷，容量負荷といった力学的因子によって引き起こされ[15]，さらに血管内皮細胞に作用する，ずり応力(シェアストレス)と細胞膜の伸展が細胞機能に重要な作用を与えている[16]。

細胞にかかるメカニカルストレスの理解と，その細胞応答のメカニズムの解析が進めば，メカニカルストレスが引き起こす循環器系の疾患の治療法が開発されることが期待される。

1. 心肥大

出生後，分化した心筋細胞は分裂能を失ってしまう。そのため機械的刺激が高くなると，心筋細胞は細胞の容積を増すことで，心臓にかかる単位面積当たりの力学的負荷を減少させる[15]。つまり，心肥大は心臓にかかる負荷を正常値に保つための適応反応であるが，過剰な負荷の連続は心不全を引き起こすことが知られている[17]。心肥大の作用機序を解明することは，種々の心疾患に対する治療法開発のうえで重要である。

心筋細胞は，心肥大の際にタンパク質の構造を変